J. Fluid Mech. (1993), *vol.* 257, *pp.* 1–31

Two-fluid viscous flow in a corner

By D. M. ANDERSON† AND S. H. DAVIS
Department of Engineering Sciences and Applied Mathematics, Northwestern University, Evanston, IL 60208, USA

(Received 27 October 1992 and in revised form 25 May 1993)

We consider steady, two-dimensional viscous flow of two fluids near a corner. The two fluids meet at the wedge vertex and are locally in contact with each other along a straight line emanating from the corner. The double wedge, treated in polar coordinates, admits separable solutions with bounded velocities at the corner. We seek *local solutions* which satisfy all local boundary conditions, as well as *partial local solutions* which satisfy all but the normal-stress boundary conditions. We find that local solutions exist for a wide range of total wedge angles and that a class of individual wedge angles and stress exponents is selected. Partial local solutions exist for all combinations of individual wedge angles and the stress exponents are determined as functions of these angles and the viscosity ratio. In both cases, Moffatt vortices can be found. Our aim in this work is to describe local two-fluid flow by determining for which wedge angles solutions exist, identifying singularities in the stress at the corner, and identifying conditions under which Moffatt vortices can be present in the flow. Furthermore, for the single-wedge geometry, we identify for small capillary number non-uniformities present in solutions valid near the corner.

1. Introduction

There are many viscous flows in which the fluid must negotiate corners (e.g. flow in a driven cavity or flow over a rectangular cylinder); this is always the case in contact-line problems (Hasimoto & Sano 1980; Pan & Acrivos 1967). Near a contact line, there is a flow in a wedge, one of whose sides is a rigid boundary and the other of which is a free surface. If the contact line is stationary, it is a site of an integrable flow singularity (Davis 1983). If the contact line is moving along the solid, then it is the site of a non-integrable singularity unless the no-slip condition is effectively relaxed (Dussan V. & Davis 1974). Stationary contact lines are present in die swell and various meniscus problems. Moving contact lines are present in wetting and spreading flows. Contact-line problems are usually treated as single-fluid systems in which the second fluid is regarded as a passive gas. However, if the dynamics of both fluids is important, one should consider flow in a double-wedge region.

The local analysis of two-dimensional viscous flow of a single fluid in corner regions has been studied by several authors. Dean & Montagnon (1949) considered a wedge bounded by two rigid planes and determined the properties of the flow as functions of the wedge angle. Michael (1958) considered a wedge with one solid boundary and one planar free surface and found that in order for the free surface to be stress-free the wedge angle must be π. It is the requirement of zero normal stress on the free surface that selects a specific wedge angle. Moffatt (1964*a*) considered these cases as well as

† Present address: Department of Applied Mathematics and Theoretical Physics, University of Cambridge, Silver Street, Cambridge CB3 9EW, UK.

the case of a wedge bounded by two free surfaces and described in detail situations in which sequences of corner eddies, now known as Moffatt vortices, may be present in the flow.

These flows are local and must be matched to some outer flow (e.g. see Moffatt 1964*b*). Other studies have imbedded these local solutions in global flows. Schultz & Gervasio (1990) performed a numerical study of the die swell problem with special attention drawn to the singularity at the die exit. Their treatment of the problem is the first numerical study consistent with the local predictions of the separation angle made by Michael (1958). For zero surface tension they find that the separation angle is π. When they considered non-zero surface tension, they found that the separation angle is not 180°, but argue that this is not in violation of the local analysis since the free-surface curvature has the same singular form as the normal stress. Richardson (1970) considered the 'stick-slip' problem in a two-dimensional channel. This problem is similar to the die swell problem in that at a point along the channel the boundary condition abruptly changes from a no-slip condition to a zero-shear-stress condition. The solution to this problem may be viewed as the solution to the die swell problem in the limit of infinite surface tension.

Richardson (1970) performed a regular perturbation expansion in the limit of large surface tension and suggested that the correction to the die swell exit angle violates Michael's local solution since it required that a planar free surface meet a planar rigid boundary at an angle other than π. We perform a regular perturbation expansion similar to that of Richardson. However, in our local expansion we impose no far-field boundary conditions and hence the position of the free surface remains undetermined. In this way we are able to identify non-uniformities present in the expansion for exit angles near π as the corner is approached. This analysis confirms the suggestion by Richardson that singular methods must be used in order to obtain a uniformly valid solution. We demonstrate that the expansion by Richardson breaks down as the corner is approached. Therefore, it is not a local solution and the result of Michael should not apply. In support of the results of Schultz & Gervasio (1990), we show that the actual local solution valid for $r \to 0$ has infinite curvature which balances the normal force along the free surface. In the die swell problem, then, we can imagine that this local solution can be matched with the result given by Richardson for some larger value of r.

Proudman & Asadullah (1988) have treated the case of two fluids meeting along a horizontal rigid plane. They discovered that the inclusion of the second fluid in the limit of vanishing viscosity ratio between the two fluids introduces a new mode of flow not present in the single-fluid model. Michael & O'Neill (1977) considered a double-wedge geometry with variable total angle but with the same fluid in each wedge. This is the situation of single-fluid flow in a wedge with a separating streamline emanating from the wedge vertex. The object of the present work is to extend these analyses to include all double-wedge configurations for all viscosity ratios. Such situations are present in various processing systems, for example, Czochralski and other meniscus-defined crystal growth configurations.

In the present work we shall seek both *local solutions*, those that satisfy *all* local boundary conditions, and *partial local solutions*, those that, when free surfaces are present, satisfy all local boundary conditions with the exception of the normal-stress boundary condition. Partial local solutions are important in the description of the local flow valid for infinite surface tension (or zero capillary number). When perturbation methods for small capillary number are used, conditions on the flow imposed by the normal-stress boundary condition do not appear in the leading-order problem and

therefore partial local solutions can be viewed as leading-order solutions for these cases. Partial local solutions also describe cases in which there exists an appropriate spatially varying pressure distribution outside the free surface such that the normal-stress boundary condition is satisfied without further restriction on the flow (Moffatt 1964*a*). Under such an assumption, the restriction of small capillary number is not necessary. When such provisions are made for the pressure, these solutions satisfy all local boundary conditions and can be thought of as specialized local solutions. Trogdon & Joseph (1981) study the singularity at the exit in the die swell problem for values of surface tension not necessarily large. They examined the singularity through a local analysis similar to that of Moffatt (1964*a*), and determined the stress exponent as a function of surface tension by solving the local problem without the kinematic boundary condition, the condition in their analysis that determines the position of the free surface. This is a different type of partial local solution but the spirit of the analysis is the same as those motivated by large surface tension.

The present work seeks to extend the single-fluid cases, the double-wedge system studied by Michael & O'Neill (1977), and the two-fluid system for a horizontal plate studied by Proudman & Asadullah (1988) to the case of general viscosity ratios and general angles for two-fluid systems. In §2 we shall analyse the non-uniformities present in the small capillary number expansion for a single wedge and review the single-fluid results. We then extend these ideas in §3 to the two-fluid problem. We shall consider the class of solutions that have bounded velocities at the wedge vertex.

2. Single-fluid flow

Consider steady-two-dimensional flow in a wedge. The flow of an incompressible Newtonian fluid is governed by the Navier–Stokes equations. Such a flow can be characterized by the Reynolds number $R = \rho U r/\mu$, where U is a velocity scale, r is a lengthscale, and ρ and μ are the density and viscosity of the fluid, respectively. The analysis of the local flow near a corner region can be simplified by defining a Reynolds number based on the distance, r, to the corner which can be taken arbitrarily small. Thus, we consider Stokes flow. This approximation is therefore valid for

$$r \ll \mu/\rho U. \tag{2.1}$$

The local flow is governed by

$$\nabla \cdot \boldsymbol{u} = 0, \tag{2.2}$$

$$\nabla \cdot \boldsymbol{\sigma} = 0, \tag{2.3}$$

where $\boldsymbol{u}$ is the velocity vector, $\boldsymbol{\sigma} = -p\boldsymbol{I} + \mu[\nabla \boldsymbol{u} + (\nabla \boldsymbol{u})^{\mathrm{T}}]$ is the stress tensor, and p is the pressure. A stream function, ψ, defined in plane polar coordinates, where

$$\boldsymbol{u} = \left(\frac{1}{r}\frac{\partial \psi}{\partial \theta}, -\frac{\partial \psi}{\partial r}\right) \tag{2.4}$$

satisfies the biharmonic equation

$$\nabla^4 \psi = 0. \tag{2.5}$$

In polar coordinates the biharmonic equation has separable solutions of the form

$$\begin{aligned}\psi = {} & r^{\sigma+1}\{A_\sigma \cos(\sigma+1)\theta + B_\sigma \sin(\sigma+1)\theta + C_\sigma \cos(\sigma-1)\theta + D_\sigma \sin(\sigma-1)\theta\} \\ & + r^2(A_1 \cos 2\theta + B_1 \sin 2\theta + C_1\theta + D_1) + r(A_0 \cos\theta + B_0 \sin\theta + C_0\theta\cos\theta + D_0\theta\sin\theta),\end{aligned} \tag{2.6}$$

where A_i, B_i, C_i, D_i for $i = 0, 1, \sigma$ ($\sigma \neq 0, 1$) are unknown constants to be determined by the boundary conditions. In general, one or more of these coefficients will be left

	$\theta = 0$	$\theta = \alpha$
rr	rigid	rigid
rf	rigid	free
ff	free	free

TABLE 1. Summary of wedge cases considered

undetermined by the local analysis; these are in principle determined by matching to an outer flow. The exponent σ, which arises as a separation constant, may be complex and is taken to have positive real part. Values of σ with $\mathrm{Re}(\sigma) < 0$ are not considered since they lead to unbounded velocities at the wedge vertex, $r = 0$. For similar reasons, solutions of the biharmonic equation such as $\ln r$, $r^2 \ln r, \theta \ln r$, and $\theta r^2 \ln r$ have also been excluded here.

Boundary conditions along the two wedge boundaries determine the constants in (2.6) and also may impose certain restrictions on the values of σ and wedge angle α. Along a rigid surface, both velocity components must vanish. Along a planar free surface, the normal velocity and the shear and normal stresses must vanish. The azimuthal component of the velocity must vanish. on the free surface. Also, the shear stress vanishes,

$$(\boldsymbol{\sigma} \cdot \boldsymbol{n}) \cdot \boldsymbol{t} = 0, \tag{2.7}$$

where $\boldsymbol{n}$ and $\boldsymbol{t}$ are the unit normal vector (directed outward from the wedge) and unit tangent vector to the surface, respectively. If we examine the normal-stress boundary condition, we have, in dimensionless form,

$$(\boldsymbol{\sigma} \cdot \boldsymbol{n}) \cdot \boldsymbol{n} = -\frac{1}{C}(\nabla \cdot \boldsymbol{n}), \tag{2.8}$$

where $C = U\mu/\gamma$ is the capillary number relating viscous forces on the interface to the constant value of the surface tension coefficient, γ. The free surface is taken to have zero curvature. Hence, for non-zero C the normal stress must vanish on the free surface. We shall refer to the solutions satisfying all of the boundary conditions on the free surface as *local solutions*. However, it is often the case in contact-line problems that C is a small number (Davis 1983). In the limit $C \to 0$ one can seek solutions as perturbation expansions in small capillary number (e.g. see Richardson 1970). In this limit the normal-stress boundary conditions places no restrictions on the flow field to leading order. That is, the leading-order normal stress boundary condition states only that the free surface must have zero curvature. For these cases the stream function is given by $\psi = \tilde{\psi} + O(C)$ where the zero-normal-stress requirement is not placed on $\tilde{\psi}$. We refer to such solutions, $\tilde{\psi}$, as *partial local solutions*. Moffatt (1964*a*) arrives at the same type of solution but through the assumption that there exists an appropriate spatially varying pressure field outside the free surface such that the normal-stress boundary condition is satisfied. Under such an assumption, the restriction of small capillary number is not necessary.

The wedge geometry has the azimuthal angle, θ, ranging from 0 to α and the radial distance, r, measured from the corner. The cases considered are summarized in table 1. The boundary conditions applied on a rigid plane are

$$\psi = \frac{\partial \psi}{\partial \theta} = 0. \tag{2.9}$$

These correspond to vanishing normal and tangential velocities on the rigid plane. The boundary conditions applied on a planar free surface are

$$\psi = 0, \tag{2.10a}$$

$$\frac{\partial^2 \psi}{\partial \theta^2} = 0, \tag{2.10b}$$

$$-p + \frac{2\mu}{r}\left(\frac{1}{r}\frac{\partial \psi}{\partial \theta} - \frac{\partial^2 \psi}{\partial r\, \partial \theta}\right) = 0. \tag{2.10c}$$

When the stream function is given by (2.6), the pressure takes the form

$$\frac{p}{\mu} = 4\sigma r^{\sigma-1}\{D_\sigma \cos(\sigma-1)\theta - C_\sigma \sin(\sigma-1)\theta\} + \frac{2}{r}\{C_0 \cos\theta + D_0 \sin\theta\} + 4C_1 \ln r. \tag{2.11}$$

The boundary conditions (2.10) correspond to zero normal velocity, zero shear stress and zero normal stress on the free surface, respectively. The shear and normal stresses, corresponding to the stream function given by (2.6) are

$$\begin{aligned}\mu^{-1}(\boldsymbol{\sigma}\cdot\boldsymbol{n})\cdot\boldsymbol{t} = {} & -2\sigma r^{\sigma-1}\{(\sigma+1)(A_\sigma \cos(\sigma+1)\theta + B_\sigma \sin(\sigma+1)\theta) \\ & + (\sigma-1)(C_\sigma \cos(\sigma-1)\theta + D_\sigma \sin(\sigma-1)\theta)\} \\ & - 4\{A_1 \cos 2\theta + B_1 \sin 2\theta\} + \frac{2}{r}\{D_0 \cos\theta - C_0 \sin\theta\},\end{aligned} \tag{2.12a}$$

and

$$\begin{aligned}\mu^{-1}(\boldsymbol{\sigma}\cdot\boldsymbol{n})\cdot\boldsymbol{n} = {} & 2\sigma(\sigma+1) r^{\sigma-1}\{A_\sigma \sin(\sigma+1)\theta - B_\sigma \cos(\sigma+1)\theta \\ & + C_\sigma \sin(\sigma-1)\theta - D_\sigma \cos(\sigma-1)\theta\} - 4C_1 \ln r \\ & - \frac{2}{r}\{C_0 \cos\theta + D_0 \sin\theta\} - 2\{C_1 - 2A_1 \sin 2\theta + 2B_1 \cos 2\theta\}.\end{aligned} \tag{2.12b}$$

The terms of most interest in these expressions are those corresponding to the strongest contribution near $r = 0$. These correspond to r^{-1}, $\ln r$, or $r^{\sigma-1}$ depending on whether or not the coefficient multiplying each of these terms vanishes. When the stress has the form $r^{\sigma-1}$ we are most interested in the smallest value of $\mathrm{Re}(\sigma)$. These expressions show which terms in the stream function lead to the most singular behaviour in the stress at the wedge vertex.

We shall first discuss the small-capillary-number expansion for a rigid-free wedge and then discuss the cases shown in table 1.

2.1. *Non-uniformities for small capillary number*

The following analysis identifies the type of non-uniformity in the expansions for the stream function and free-surface position for small capillary number, $C = U\mu/\gamma$ (or large surface tension, γ), for a *single wedge* with fluid of viscosity, μ, bounded by a rigid plane, $\theta = 0$, and a free surface, $\theta = \alpha(r)$. The free-surface position is not assumed planar here. This analysis offers a resolution to the seemingly contradictory results found by Richardson (1970), in his expansion for large surface tension, and Michael (1958). We perform a regular perturbation expansion for $C \ll 1$ local to the corner. This analysis is similar to that given by Richardson but in the present case we make no assumptions about the far-field conditions and therefore the free-surface position

is left undetermined by this local analysis. As a result, it is possible to identify non-uniformities which are present as the angle π is approached. We expand as follows:

$$\psi \sim \hat{\psi} + C\psi_1 + C^2\psi_2 + \ldots, \tag{2.13a}$$

$$\alpha \sim \alpha_0 + C\alpha_1 + C^2\alpha_2 + \ldots. \tag{2.13b}$$

The governing equations are the biharmonic equation for ψ with boundary conditions requiring that both velocity components vanish on $\theta = 0$, and that the normal component of the velocity vanish, the shear stress vanish, and the normal stress balances surface tension times curvature on the free surface $\theta = \alpha(r)$. Note that, since the free surface is not assumed to be planar, the boundary conditions on $\theta = \alpha(r)$ are more complicated than those given by (2.10).

At leading order we find that α_0 is constant and as a result the solution for $\tilde{\psi}$ is given by (2.28)–(2.30), (2.32) or (2.22) depending on the value of α_0.

If we include higher orders, we find that

$$\alpha \sim \alpha_0 + C\left\{\frac{a_\sigma(\alpha_0)}{\sigma(\sigma+1)} r^\sigma\right\} + C^2\left\{\frac{b_\sigma(\alpha_0)}{2\sigma(2\sigma+1)} r^{2\sigma}\right\} + \ldots, \tag{2.14}$$

where

$$a_\sigma(\alpha_0) = \frac{-4\sigma^2 D_\sigma \sin\alpha_0}{\sin\sigma\alpha_0}, \tag{2.15a}$$

$$b_\sigma(\alpha_0) = \frac{-64\sigma^2(2\sigma+1)\,D_\sigma^2}{(\sigma+1)^2\sin^2\sigma\alpha_0(2\sigma\sin 2\alpha_0 - \sin 4\sigma\alpha_0)}\{\sigma^2(\sigma^2-1)\sin^4\alpha_0 + (\sin 2\sigma\alpha_0 - 1)(\sigma^2\sin^2\alpha_0 - \sin^2\sigma\alpha_0)\}. \tag{2.15b}$$

and σ satisfies $\sigma\sin 2\alpha_0 - \sin 2\sigma\alpha_0 = 0$. The correction to the stream function has $\psi_1 \sim r^{2\sigma+1}$. The expression (2.14) is valid near but not at $\alpha_0 = \pi$.

When $\alpha_0 = \pi$,

$$\alpha \sim \pi + C\left\{a_1 + \frac{4(-1)^\sigma D_\sigma}{\sigma+1} r^\sigma\right\} + C^2 a_2 + \ldots, \tag{2.16}$$

where $\sigma = 2, 3, 4, \ldots$ and a_1 and a_2 are undetermined constants. The expansion found by Richardson (1970) corresponds to the leading-order and first-correction terms shown here where a_1 is determined by the far field. Since $\sigma = 2, 3, 4, \ldots$, this expansion corresponds to a planar interface at an angle $\alpha \sim \pi + Ca_1 + C^2a_2 + \ldots$ at $r = 0$. Such an expansion, as noted by Richardson, would violate the local results of Michael (1958) since it requires that a planar rigid surface and a planar free surface meet at an angle other than π. Further, for $\alpha_0 = \pi$, $\tilde{\psi} \sim r^{\frac{3}{2}}$ and $\psi_1 \sim r^2$. Note that a_1 and a_2 do not appear for general values of α_0 owing to solvability conditions in the higher-order problems.

To understand how the expansion obtained by Richardson breaks down we expand the solution for α given by (2.14) for α_0 near π. This gives

$$\alpha \sim \alpha_0 + C\left\{\frac{4}{3}D_{\frac{1}{2}}(\alpha_0 - \pi)\, r^{\frac{1}{2}} + \frac{4}{3}D_2 r^2 + \ldots\right\} + C^2\left\{-\frac{32}{9}D_{\frac{1}{2}}^2 \frac{r}{(\alpha_0-\pi)} + \ldots\right\} + \ldots. \tag{2.17}$$

From this equation we can identify non-uniformities for small C as r and $\alpha_0 - \pi$ approach zero; depending on how this limit is taken, different results are obtained.

Consider the case where we first let $r \to 0$ (before $\alpha_0 \to \pi$). Here we find

$$\alpha \sim \pi + C\left\{\frac{4}{3}D_{\frac{1}{2}}(\alpha_0 - \pi)\, r^{\frac{1}{2}}\right\} + C^2\left\{-\frac{32}{9}D_{\frac{1}{2}}^2 \frac{r}{(\alpha_0-\pi)}\right\} + \ldots. \tag{2.18}$$

In this limit we find that the free surface has infinite curvature at the corner. This is a valid local solution which does not violate the results presented by Michael (1958). It requires for asymptocity that $(\alpha_0-\pi) \gg C^{\frac{1}{3}}r^{\frac{1}{3}}$ so $\alpha_0 = \pi$ only if $C = 0$ or $r = 0$.

If we now reverse the order in which we take the limits by first letting $\alpha_0 \to \pi$ and then letting $r \to 0$, we find

$$\alpha \sim \pi + (\alpha_0 - \pi) + C\left\{\frac{4}{3}D_2 r^2\right\} + C^2\left\{-\frac{32}{9}D_{\frac{1}{2}}^2 \frac{r}{(\alpha_0-\pi)} + \ldots\right\} + \ldots. \tag{2.19}$$

Here we observe that the expansion is valid when $C^2 r/(\alpha_0-\pi) \ll Cr^2$, or $r \gg C/(\alpha_0-\pi)$. Therefore, as indicated by this inequality, $r \to 0$ is not allowed unless $C = 0$. Consequently, in this limit the expansion shown cannot be considered local.

This shows that while the interface calculated by Richardson does approach the corner as a plane at an angle other than π *it is not* a valid local (or inner) solution as $r \to 0$ but rather should be viewed as an intermediate expansion valid between an outer solution and an inner solution.

The above analysis shows that singular methods with the appropriate matching conditions must be used in order to obtain a uniformly valid expansion in these regimes. It also demonstrates the importance of partial local solutions in such cases.

2.2. *Rigid/rigid wedge*

Local solutions were obtained by Dean & Montagnon (1949) who sought a stream function of the form given in (2.6) but did not include the special terms $\psi \sim r, r^2$. The boundary conditions on the rigid surface, $\theta = 0, \alpha$, are given in (2.9). They found that non-trivial solutions exist only when

$$\sigma \sin\alpha \pm \sin\sigma\alpha = 0. \tag{2.20}$$

The two roots correspond to symmetric $(-)$ and antisymmetric $(+)$ modes (Moffatt 1964*a*). We note that terms in the stream function proportional to r^2 are permitted for specific wedge angles, α^*, where

$$\sin\alpha^*(\sin\alpha^* - \alpha^*\cos\alpha^*) = 0. \tag{2.21}$$

This expression can be obtained from (2.20) asymptotically for $\sigma \to 1$. There are three solutions to (2.21) on the interval $(0, 2\pi]$ given by $\alpha^* = \pi$, $\alpha^* \approx 1.43\pi$, and $\alpha^* = 2\pi$.

For $\alpha \neq \alpha^*$ the stream function is given by

$$\psi = \frac{2D_\sigma r^{\sigma+1}}{(\sigma+1)\sin\sigma\alpha\sin\alpha} g(\theta, \alpha, \sigma), \tag{2.22}$$

where

$$\frac{g(\theta,\alpha,\sigma)}{\sin\sigma\alpha\sin\alpha} \equiv \frac{\sin(\alpha-\theta)}{\sin\alpha}\sin\sigma\theta - \frac{\sin\sigma(\alpha-\theta)}{\sin\sigma\alpha}\sigma\sin\theta \tag{2.23}$$

and σ is given by (2.20).

For $\alpha = \pi, 2\pi$

$$\psi = r^{\sigma+1}\left\{2C_\sigma \sin\sigma\theta\sin\theta + \frac{2}{\sigma+1}D_\sigma(\sin\sigma\theta\cos\theta - \sigma\cos\sigma\theta\sin\theta)\right\}, \tag{2.24}$$

where $\sigma = 1, 2, 3, 4, \ldots$, for $\alpha = \pi$ and $\sigma = \frac{1}{2}, 1, \frac{3}{2}, 2, \ldots$, for $\alpha = 2\pi$. Note here that the case $\sigma = 1$ gives the correct r^2 term in the stream function so we have combined the cases for simplicity.

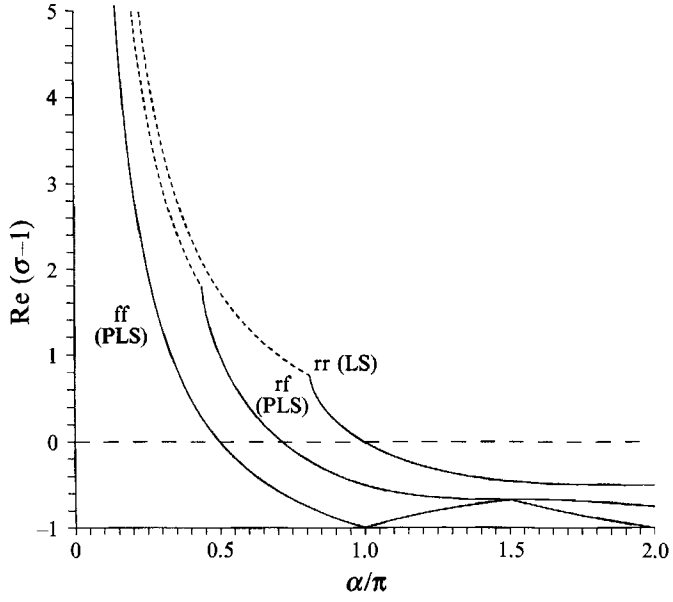

FIGURE 1. The real part, $\mathrm{Re}(\sigma-1)$, of the most dominant stress exponent, for three different types of hydrodynamic boundary conditions: rigid/rigid wedge (rr) for local solutions (LS) (Dean & Montagnon 1949), and rigid/free wedge (rf) and free/free wedge (ff) for partial local solutions (PLS) (Moffatt 1964*a*). The stress field is singular when this exponent is negative. There are logarithmic singularities present when $\alpha \approx 1.43\pi$ in the rigid/rigid case and when $\alpha \approx 0.715\pi$, 1.23π, and 1.74π in the rigid/free case. No logarithmic singularities are present in the free/free case. The dashed portions of the curves indicate that the root has a non-zero imaginary part; the root is complex for $\alpha < 0.813\pi$ in the rigid/rigid case and for $\alpha < 0.441\pi$ in the rigid/free case. The free/free wedge root, including all higher modes, is always real.

For $\alpha = \alpha^* \approx 1.43\pi$

$$\psi = \frac{2D_\sigma r^{\sigma+1}}{(\sigma+1)\sin\sigma\alpha^* \sin\alpha^*} g(\theta, \alpha^*, \sigma) + B_1 r^2(\alpha^* - 2\theta - \alpha^* \cos 2\theta + \sin 2\theta), \quad (2.25)$$

where σ is given by (2.20).

Figure 1 shows a plot of the smallest positive value of $\mathrm{Re}(\sigma-1)$ as a function of α (Dean & Montagnon 1949). For general α the stress field has radial dependence given by $r^{\sigma-1}$ so that the corner is the location of a singular stress field for wedge angles exceeding π. However, the stress field is integrable for all wedge angles. For $\alpha \approx 1.43\pi$ there is a logarithmic singularity in the stress, though this is not the dominant singularity. The exponent σ becomes complex for $\alpha < 0.813\pi$ giving rise to corner eddies in the flow as described by Moffatt (1964*a*).

2.3. *Rigid/free wedge*

Here the rigid boundary is at $\theta = 0$ and the free surface is at $\theta = \alpha$. Michael (1958) solved the biharmonic equation using the same separable form for the stream function as used by Dean & Montagnon (1949) and imposed the boundary conditions given by (2.9) on $\theta = 0$ and (2.10) on $\theta = \alpha$. Notice that there are now five boundary conditions rather than four. Since the interface is taken to be planar, the 'extra' boundary condition, the normal-stress boundary condition, determines α, the position of the free

surface. Michael (1958) has shown that in order for a non-trivial solution to exist, the wedge angle must be π. The local solutions are then given by

$$\psi = -2A_\sigma r^{\sigma+1} \sin\sigma\theta \sin\theta, \quad \sigma = \tfrac{1}{2}, \tfrac{3}{2}, \tfrac{5}{2}, \ldots. \tag{2.26}$$

Here the stress field has a square-root singularity at the contact line $r = 0$. The more general form of the stream function, given by (2.6) does not lead to additional terms in the solution.

For partial local solutions, the leading-order stream function, $\tilde{\psi}$, is found by imposing all of the above boundary conditions except for the normal-stress boundary condition. The result is that non-trivial solutions for $\tilde{\psi}$ can be found for all wedge angles with the value of σ determined by

$$\sigma \sin 2\alpha - \sin 2\sigma\alpha = 0. \tag{2.27}$$

As noted by Moffatt (1964*a*), this result can be obtained by using the symmetric mode of (2.20) in a wedge of angle 2α. This result (e.g. Moffatt 1964*a*; Brown 1991) provides a means of determining σ and hence the singular nature of the flow as a function of the wedge angle. The leading-order stream function is given as follows:

for $\alpha = \frac{1}{2}\pi$

$$\tilde{\psi} = r^{\sigma+1} \begin{cases} \dfrac{2}{\sigma+1} \tilde{D}_\sigma (\sin\sigma\theta\cos\theta - \sigma\cos\sigma\theta\sin\theta), & \sigma = 3, 5, 7, \ldots \\ -2\tilde{A}_\sigma \sin\sigma\theta\sin\theta, & \sigma = 2, 4, 6, \ldots, \end{cases} \tag{2.28}$$

for $\alpha = \pi$

$$\tilde{\psi} = r^{\sigma+1} \begin{cases} \dfrac{2}{\sigma+1} \tilde{D}_\sigma (\sin\sigma\theta\cos\theta - \sigma\cos\sigma\theta\sin\theta), & \sigma = 2, 3, 4, \ldots \\ -2\tilde{A}_\sigma \sin\sigma\theta\sin\theta, & \sigma = \tfrac{1}{2}, \tfrac{3}{2}, \tfrac{5}{2}, \ldots, \end{cases} \tag{2.29}$$

for $\alpha = \frac{3}{2}\pi$

$$\tilde{\psi} = r^{\sigma=1} \begin{cases} \dfrac{2}{\sigma+1} \tilde{D}_\sigma (\sin\sigma\theta\cos\theta - \sigma\cos\sigma\theta\sin\theta), & \sigma = \tfrac{1}{3}, \tfrac{5}{3}, \tfrac{7}{3}, \ldots \\ -2\tilde{A}_\sigma \sin\sigma\theta\sin\theta, & \sigma = \tfrac{2}{3}, \tfrac{4}{3}, 2, \ldots. \end{cases} \tag{2.30}$$

The case $\alpha = \pi$ coincides with the 'stick-slip' analysis of Richardson (1970).

Additional terms in the stream function proportional to r^2 are allowed for wedge angles, α_c, satisfying

$$\sin 2\alpha_c - 2\alpha_c \cos 2\alpha_c = 0. \tag{2.31}$$

This equation can be obtained from (2.27) asymptotically for $\sigma \to 1$. There are three solutions to (2.31) on the interval $(0, 2\pi)$ which are given approximately by 0.715π, 1.23π, and 1.74π. Here the stream function is given by

$$\tilde{\psi} = \frac{2\tilde{D}_\sigma r^{\sigma+1}}{(\sigma+1)\sin\sigma\alpha_c \sin\alpha_c} g(\theta, \alpha_c, \sigma) + \tilde{B}_1 r^2 (2\alpha_c - 2\theta - 2\alpha_c \cos 2\theta + \sin 2\theta), \tag{2.32}$$

where σ satisfies (2.27).

For $\alpha \neq \frac{1}{2}\pi, \pi, \frac{3}{2}\pi, \alpha_c$ the stream function is given by (2.22) with values of σ satisfying (2.27).

The local behaviour of the flow is dominated by the term corresponding to the smallest value of $\mathrm{Re}(\sigma)$. For $\alpha = \frac{1}{2}\pi$ the flow is regular, for $\alpha = \pi$ there is a square-root singularity in the stress, and for $\alpha = \frac{3}{2}\pi$ the stress is singular ($\sim r^{-\frac{2}{3}}$). For general α

figure 1 shows a plot of $\mathrm{Re}(\sigma-1)$ *vs.* α where σ is the root of (2.27) with the smallest real part. We see that the stress is singular for $\alpha > 0.715\pi$ but is always integrable. When $\alpha = \alpha_c$ a logarithmic stress singularity is present (see (2.12*b*)). However, this is the dominant singularity only when $\alpha_c = 0.715\pi$, the point where σ passes through unity. Notice that σ becomes complex for values of $\alpha < 0.441\pi$, indicating the presence of Moffatt vortices (Moffatt 1964*a*). These vortices, however, are only present in the partial local solutions; they are not present for local solutions.

2.4. *Free/free wedge*

Local solutions, satisfying boundary conditions (2.10) on $\theta = 0, \alpha$, can only be found for the specific wedge angle $\alpha = \pi$. Here we find that

$$\psi = 2B_\sigma r^{\sigma+1}\cos\sigma\theta\sin\theta + B_0 r\sin\theta, \quad \sigma = 2,3,4,\ldots. \tag{2.33}$$

Notice that the 'wedge' is just a flat surface when $\alpha = \pi$. Not surprisingly the flow is regular.

Next we consider partial local solutions. Moffatt (1964*a*) showed the results for antisymmetric flows. For completeness we present all of the possibilities here.

The existence of partial local solutions requires that

$$\sin(\sigma+1)\alpha\sin(\sigma-1)\alpha = 0. \tag{2.34}$$

For $\alpha \neq \frac{1}{2}\pi, \pi, \frac{3}{2}\pi$ we have

$$\tilde{\psi} = r^{\sigma+1}\begin{cases}\tilde{D}_\sigma\sin(\sigma-1)\theta, & \sigma = m\pi/\alpha+1\\ \tilde{B}_\sigma\sin(\sigma+1)\theta, & \sigma = m\pi/\alpha-1,\end{cases} \tag{2.35}$$

where m is any non-zero integer (positive or negative) such that $\sigma > 0$ and $\sigma \neq 1$. As noted by Moffatt 1964*a*), the exponent is *always* real and hence no eddies are present for wedges defined by two free surfaces. The smallest exponent, $\sigma-1$, corresponding to the locally dominant stress field, is plotted as a function of α in figure 1. Note that the smallest value of $\sigma-1$ corresponds to three separate branches of (2.34). The stress field is singular for $\alpha > \frac{1}{2}\pi$ but is always integrable.

For $\alpha = \frac{1}{2}\pi$,

$$\tilde{\psi} = r^{\sigma+1}\{\tilde{B}_\sigma\sin(\sigma+1)\theta + \tilde{D}_\sigma\sin(\sigma-1)\theta\} + \tilde{B}_1 r^2\sin 2\theta, \quad \sigma = 3,5,7,\ldots. \tag{2.36}$$

For $\alpha = \pi$,

$$\tilde{\psi} = r^{\sigma+1}\{\tilde{B}_\sigma\sin(\sigma+1)\theta + \tilde{D}_\sigma\sin(\sigma-1)\theta\} + B_1 r^2\sin 2\theta + \tilde{B}_0 r\sin\theta, \quad \sigma = 2,3,4,\ldots. \tag{2.37}$$

For $\alpha = \frac{3}{2}\pi$,

$$\tilde{\psi} = r^{\sigma+1}\{\tilde{B}_\sigma\sin(\sigma+1)\theta + \tilde{D}_\sigma\sin(\sigma-1)\theta\} + \tilde{B}_1 r^2\sin 2\theta, \quad \sigma = \tfrac{1}{3},\tfrac{5}{3},\tfrac{7}{3},3,\ldots. \tag{2.38}$$

For $\alpha = \frac{1}{2}\pi$ and π the flow is regular. When $\alpha = \frac{3}{2}\pi$ the stress is singular ($\sim r^{-\frac{2}{3}}$).

In figure 1 a comparison between the exponents for the local solutions in the rigid/rigid case, and the partial local solutions in the rigid/free and free/free cases can be made. First, we see that the rigid/rigid wedge is the least singular case while the free/free case is the most singular. Second, for all three cases, larger wedges tend to have stronger singularities, however, in the free/free case σ increases on the interval $(\pi, \frac{3}{2}\pi)$. Finally, we note that in all three cases $\mathrm{Re}(\sigma)\to\infty$ as $\alpha\to 0$ indicating that the flow near the corner becomes weaker as the angle becomes smaller. Moffatt vortices may be present whenever a rigid surface is present. However, when local solutions are sought in the rigid/free case no Moffatt vortices are found.

3. Two-fluid flow

We now consider the two-fluid system with the geometry as shown in figure 2. Here the outer boundaries are rigid planes and are given by $\theta = -\alpha_1$ and $\theta = \alpha_2$, and the interface separating the two fluids is given by $\theta = 0$; the total wedge angle is $\alpha \equiv \alpha_1 + \alpha_2$. The fluids in regions 1 and 2 are characterized by viscosities μ_1 and μ_2, respectively, with $\mu \equiv \mu_2/\mu_1$. We solve the biharmonic equation in each phase with boundary conditions

$$\psi_1 = \frac{\partial \psi_1}{\partial \theta} = 0 \quad \text{on } \theta = -\alpha_1, \tag{3.1a}$$

$$\psi_2 = \frac{\partial \psi_2}{\partial \theta} = 0, \quad \text{on } \theta = \alpha_2, \tag{3.1b}$$

$$\psi_1 = \psi_2 = 0 \quad \text{on } \theta = 0, \tag{3.1c}$$

$$\left[\frac{\partial \psi_i}{\partial \theta}\right]_{i=1}^{i=2} = 0 \quad \text{on } \theta = 0, \tag{3.1d}$$

$$\left[\mu_i\left(-\frac{\partial^2 \psi_i}{\partial r^2} + \frac{1}{r}\frac{\partial \psi_i}{\partial r} + \frac{1}{r^2}\frac{\partial^2 \psi_i}{\partial \theta^2}\right)\right]_{i=1}^{i=2} = 0, \quad \text{on } \theta = 0, \tag{3.1e}$$

$$\left[-p_i + \frac{2\mu_i}{r}\left(\frac{1}{r}\frac{\partial \psi_i}{\partial \theta} - \frac{\partial^2 \psi_i}{\partial r\, \partial \theta}\right)\right]_{i=1}^{i=2} = 0 \quad \text{on } \theta = 0. \tag{3.1f}$$

These state that the normal and tangential velocities vanish on $\theta = -\alpha_1, \alpha_2$, the normal velocities vanish on $\theta = 0$, and that the jump in the tangential velocities, shear stresses, and normal stresses vanish across the free surface at $\theta = 0$. We assume solutions of the form

$$\psi_i = r^{\sigma+1}\{A_\sigma^{(i)} \cos(\sigma+1)\theta + B_\sigma^{(i)} \sin(\sigma+1)\theta + C_\sigma^{(i)} \cos(\sigma-1)\theta + D_\sigma^{(i)} \sin(\sigma-1)\theta\} + r^2\{A_1^{(i)} \cos 2\theta + B_1^{(i)} \sin 2\theta + C_1^{(i)}\theta + D_1^{(i)}\} \tag{3.2}$$

for $i = 1, 2$ where we have excluded terms corresponding to unbounded velocities at the origin. We find that there is no contribution from terms like $\psi \sim r$.

Proudman & Asadullah (1988) considered two fluids of different viscosities for the case with total wedge angle π and described partial local solutions. The following extends their results to treat partial local solutions for total wedge angles other than π, and local solutions for all total wedge angles.

There exist partial local solutions for all wedge angles. Using the notation of Proudman & Asadullah (1988), we find that this requires

$$\{F(2\alpha_1) - F(2\sigma\alpha_1)\}\{F^2(\alpha_2) - F^2(\sigma\alpha_2)\} + \mu\frac{\alpha_1}{\alpha_2}\{F(2\alpha_2) - F(2\sigma\alpha_2)\}\{F^2(\alpha_1) - F^2(\sigma\alpha_1)\} = 0 \tag{3.3}$$

for the coefficients of $r^{\sigma+1}$, and

$$\{F(2\alpha_1) - \cos 2\alpha_1\}\{F^2(\alpha_2) - F(\alpha_2)\cos\alpha_2\} + \mu\frac{\alpha_1}{\alpha_2}\{F(2\alpha_2) - \cos 2\alpha_2\}\{F^2(\alpha_1) - F(\alpha_1)\cos\alpha_1\} = 0 \tag{3.4}$$

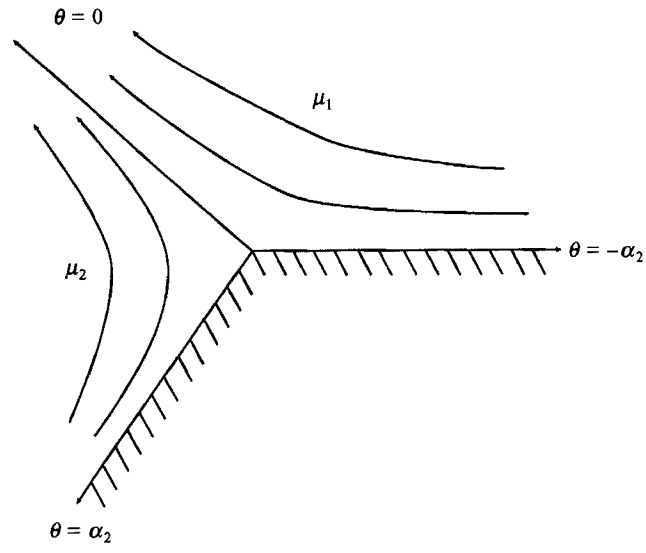

FIGURE 2. The two-fluid wedge geometry. The boundaries at $\theta = -\alpha_1$ and $\theta = \alpha_2$ are rigid while $\theta = 0$ is a planar free surface. Fluid 1 is characterized by a viscosity μ_1 and fluid 2 by a viscosity μ_2.

for the coefficients of r^2 where

$$F(z) \equiv \frac{\sin z}{z}. \tag{3.5}$$

Compare (3.3) with (1.6) in Proudman & Asadullah (1988) (take $\sigma \to \lambda$, $\alpha_1 \to \alpha$, and $\alpha_2 \to \pi - \alpha$ to obtain their result). Notice that (3.4) can be obtained from (3.3) asymptotically for $\sigma \to 1$. The relation between these two equations is analogous to that in the single-fluid cases (see (2.20) and (2.21), and (2.27) and (2.31)).

When (3.3) is satisfied, the stream functions are given by (3.2) with coefficients

$$A_\sigma^{(1)} = -\mu C_\sigma^{(2)}, \tag{3.6a}$$

$$B_\sigma^{(1)} = B_\sigma^{(2)} + \frac{\sigma - 1}{\sigma + 1}(D_\sigma^{(2)} - D_\sigma^{(1)}), \tag{3.6b}$$

$$C_\sigma^{(1)} = \mu C_\sigma^{(2)}, \tag{3.6c}$$

$$D_\sigma^{(1)} = \frac{-\mu(\sigma \sin^2 \alpha_1 + \sin^2 \sigma\alpha_1)(\sigma \sin 2\alpha_2 - \sin 2\sigma\alpha_2)}{(\sigma \sin^2 \alpha_2 + \sin^2 \sigma\alpha_2)(\sigma \sin 2\alpha_1 - \sin 2\sigma\alpha_1)} D_\sigma^{(2)}, \tag{3.6d}$$

$$A_\sigma^{(2)} = -C_\sigma^{(2)}, \tag{3.6e}$$

$$B_\sigma^{(2)} = \frac{\sigma \sin^2 \alpha_2 - \sin^2 \sigma\alpha_2}{\sigma \sin^2 \alpha_2 + \sin^2 \sigma\alpha_2} D_\sigma^{(2)}, \tag{3.6f}$$

$$C_\sigma^{(2)} = \frac{-(\sigma \sin 2\alpha_2 - \sin 2\sigma\alpha_2)}{2(\sigma \sin^2 \alpha_2 + \sin^2 \sigma\alpha_2)} D_\sigma^{(2)}, \tag{3.6g}$$

where $D_\sigma^{(2)}$ remains arbitrary. These expressions were obtained under the assumptions that $\sigma \sin 2\alpha_2 - \sin 2\sigma\alpha_2 \neq 0$, $\sigma \sin 2\alpha_1 - \sin 2\sigma\alpha_1 \neq 0$, and $\sigma \sin^2 \alpha_2 + \sin^2 \sigma\alpha_2 \neq 0$. However, with the exception of the case where $\alpha_1 = \alpha_2 = \pi$ and $\sigma = 2, 3, 4, \ldots$ the expressions for the coefficients can be obtained from (3.6) in the limits as these values are approached.

When $\alpha_1 = \alpha_2 = \pi$ and $\sigma = 1, 2, 3, 4, \ldots$, the stream functions are given by

$$\tilde{\psi}_1 = r^{\sigma+1}\left\{2\mu C_\sigma^{(2)} \sin\sigma\theta \sin\theta + \frac{2D_\sigma^{(1)}}{\sigma+1}(\sin\sigma\theta\cos\theta - \sigma\cos\sigma\theta\sin\theta)\right\}, \tag{3.7a}$$

$$\tilde{\psi}_2 = r^{\sigma+1}\left\{2C_\sigma^{(2)} \sin\sigma\theta \sin\theta + \frac{2D_\sigma^{(2)}}{\sigma+1}(\sin\sigma\theta\cos\theta - \sigma\cos\sigma\theta\sin\theta)\right\}. \tag{3.7b}$$

Note that the case $\sigma = 1$ gives the correct r^2 term so this term is not written separately.

For parameter values that also satisfy (3.4) the stream functions are given by

$$\tilde{\psi}_1 = r^{\sigma+1}\{A_\sigma^{(1)}\cos(\sigma+1)\theta + B_\sigma^{(1)}\sin(\sigma+1)\theta + C_\sigma^{(1)}\cos(\sigma-1)\theta + D_\sigma^{(1)}\sin(\sigma-1)\theta\}$$
$$+\mu r^2 A_1^{(2)}\left\{\cos 2\theta - 1 - \frac{2(1-\cos 2\alpha_1)}{\sin 2\alpha_1 - 2\alpha_1\cos 2\alpha_1}\theta - \frac{1-\cos 2\alpha_1 - 2\alpha_1\sin 2\alpha_1}{\sin 2\alpha_1 - 2\alpha_1\cos 2\alpha_1}\sin 2\theta\right\}, \tag{3.8a}$$

$$\tilde{\psi}_2 = r^{\sigma+1}\{A_\sigma^{(2)}\cos(\sigma+1)\theta + B_\sigma^{(2)}\sin(\sigma+1)\theta + C_\sigma^{(2)}\cos(\sigma-1)\theta + D_\sigma^{(2)}\sin(\sigma-1)\theta\}$$
$$+r^2 A_1^{(2)}\left\{\cos 2\theta - 1 + \frac{2(1-\cos 2\alpha_2)}{\sin 2\alpha_2 - 2\alpha_2\cos 2\alpha_2}\theta + \frac{1-\cos 2\alpha_2 - 2\alpha_2\sin 2\alpha_2}{\sin 2\alpha_2 - 2\alpha_2\cos 2\alpha_2}\sin 2\theta\right\}, \tag{3.8b}$$

where the coefficients for the terms proportional to $r^{\sigma+1}$ are given by (3.6). Although these expressions are not strictly valid when $\sin 2\alpha_1 - 2\alpha_1\cos 2\alpha_1 = 0$ or $\sin 2\alpha_2 - 2\alpha_2\cos 2\alpha_2 = 0$, the result in these cases can be recovered from these expressions in the limits as those values are approached; hence we present only the most general case.

Equations (3.3) determines the allowable values of σ for given values of α_1, α_2, and μ. This condition is analogous to conditions (2.20) and (2.27) and in fact contains as factors the single-fluid relations. Note that without loss of generality we can take $\mu \leqslant 1$. Also note that when $\alpha_1 = \alpha_2 = \frac{1}{2}\alpha$ the value of σ is independent of μ and this condition may be satisfied by a symmetric mode in a wedge of angle α or by either a symmetric mode or an antisymmetric mode in each wedge of angle $\frac{1}{2}\alpha$. We have analysed (3.3) numerically and asymptotically to find the roots, σ. Figures 3–7 show the real parts of the numerically computed roots for different values of μ and α. Again we are most interested in the root with the smallest real part.

Proudman & Asadullah (1988) found that the inclusion of the second fluid for $\mu \ll 1$ leads to two modes of flow, the 'velocity' mode, and the 'stress' mode. They noted that the limit $\mu \to 0$ must be interpreted as $\mu_1 \to \infty$ rather than $\mu_2 \to 0$ since only Stokes flows are being examined. We find that these two modes of flow are present for all angles α.

Figure 3 shows the real part of the roots, σ, for $\alpha = 2\pi$. The dashed curves represent the solution for $\mu = 0$. From (3.3) we see that solutions for $\mu \to 0$ satisfy

$$(\sigma\sin 2\alpha_1 - \sin 2\sigma\alpha_1)(\sigma^2\alpha_2 - \sin^2\sigma\alpha_2) = 0.$$

Physically, $\mu = 0$ represents flow in a single wedge bounded by a rigid plane at $\theta = -\alpha_1$ and a planar free surface at $\theta = 0$. Hence we expect that the roots, σ, satisfy $\sigma\sin 2\alpha_1 - \sin 2\sigma\alpha_1 = 0$ as in the single-fluid problem. This is the 'velocity' mode. However, the two-fluid problem has additional roots from fluid 2 satisfying $\sigma^2\sin^2\alpha_2 - \sin^2\sigma\alpha_2 = 0$. This is the 'stress' mode. The dashed curves shown for $\mu = 0$ represent the smallest value of $\mathrm{Re}(\sigma-1)$ satisfying *either* of these two equations. Therefore, the smallest value of $\mathrm{Re}(\sigma-1)$ for $\mu \to 0$ is a combination of the two separate branches whose real parts intersect.

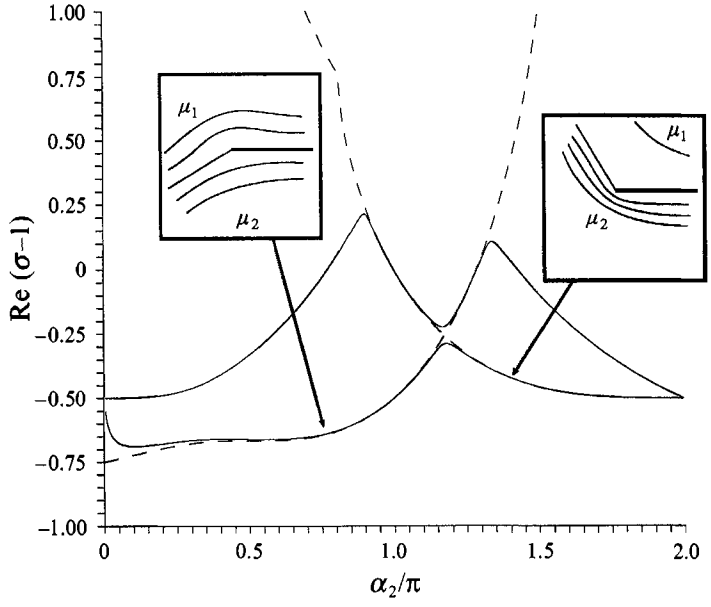

FIGURE 3. Partial local solutions: the nonlinear interaction of two solution branches for small but non-zero μ and for $\alpha = \alpha_1 + \alpha_2 = 2\pi$. The dashed curves represent segments of the solution branches for $\mu = 0$. These roots are real valued and hence the intersection shown is a true double root when $\mu = 0$. The solid curves, corresponding to $\mu = 0.01$, show the boundary-layer behaviour near the intersection. There is also boundary-layer behaviour near $\alpha_2 = 0$ in the lower roots indicating that a non-uniformity is present as both α_2 and μ approach zero. The insets show the flow field for the points indicated by arrows. The inset on the left corresponds to the velocity mode and the inset on the right corresponds to the stress mode (Proudman & Asadullah 1988).

The insets in figure 3 show sketches of the flow corresponding to the 'velocity' mode and the 'stress' mode. The left inset corresponds to the velocity mode and has non-zero velocity on the streamline separating the two fluids. The right inset corresponds to the stress mode in which the flow in wedge two is approximately flow bounded by two *rigid* planes. Fluid 1 is driven by stresses along the interface and is nearly static.

The intersection of the branches for $\mu = 0$ implies the existence of double roots, which is important for understanding the behaviour of the roots when $\mu \neq 0$. When μ is perturbed from zero, there is root splitting that occurs at the points of intersection; the roots split and form two separate branches, an upper and a lower. There are many such intersections in the solution space at which such bifurcation occurs and, in fact, the upper root in figure 3 has bifurcated in three locations. The range of values of α for which the lowest modes intersect is given approximately by $1.35\pi < \alpha \leqslant 2\pi$. Outside of this range, these roots do not intersect in the complex plane. The lower root is also non-uniform as both α_2 and μ approach zero. Owing to the nature of this splitting, we see that the dominant mode now corresponds to a single branch over the entire range of α_2. The Appendix contains a perturbation analysis that captures this root splitting and gives a uniformly valid representation of the lower root for $\mu \ll 1$. The asymptotic results agree well with the numerically computed roots in this range.

Figure 4 shows the behaviour of the lowest branch for a wider range of μ. As μ increases from zero to one, the value of $\mathrm{Re}\,(\sigma - 1)$ approaches $-\frac{1}{2}$. Note that the value of σ is independent of μ when $\alpha_1 = \alpha_2 = \frac{1}{2}\alpha$. The stress is singular for all values of μ and α_2, and all branches shown are real-valued. Figure 5 shows similar results for $\alpha = \frac{3}{2}\pi$.

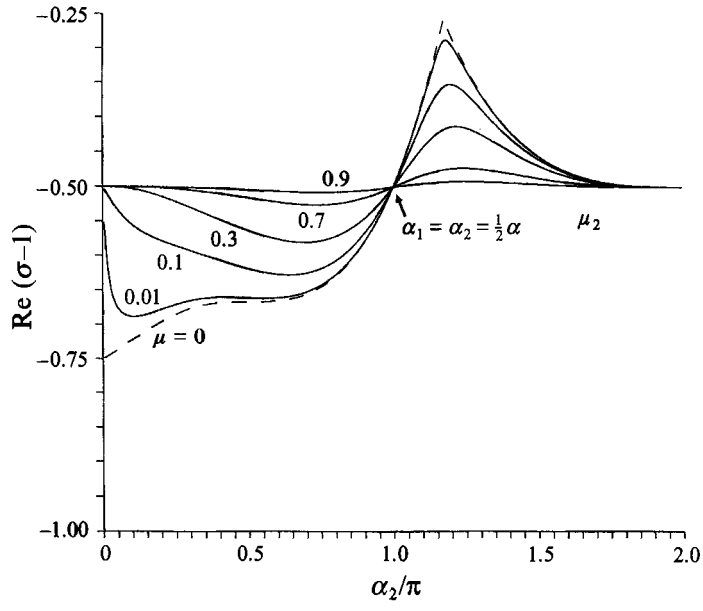

FIGURE 4. Partial local solutions: the two-fluid stress exponents of the lower branch in figure 3 for $\alpha = 2\pi$ and various viscosity ratios, μ. Note that $\mathrm{Re}\,(\sigma-1)$ is always negative and hence the stress is always singular. Also, the value of σ at $\alpha_2 = \frac{1}{2}\alpha = \pi$ is independent of the value of μ. The roots shown here have zero imaginary parts.

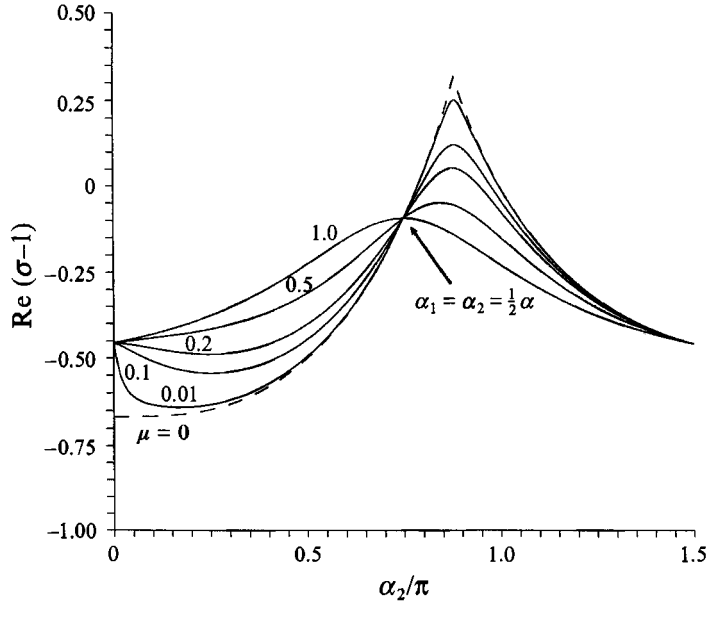

FIGURE 5. Partial local solutions; The two-fluid stress exponents for $\alpha = \frac{3}{2}\pi$ and various viscosity ratios, μ. There is a range of values with α_2 slightly larger than $\frac{1}{2}\alpha$ and μ small for which the stress is non-singular. All of the roots shown have zero imaginary parts.

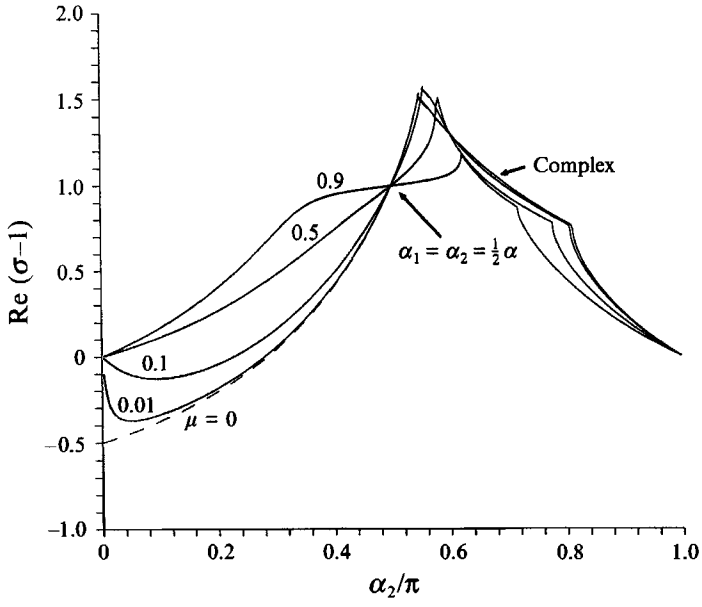

FIGURE 6. Partial local solutions: the two-fluid stress exponents for $\alpha = \pi$ and various viscosity ratios, μ. Proudman & Asadullah (1988) treated this case. Here the stress is non-singular except for small values of α_2 and μ. There is range of values of α_2 slightly greater than $\frac{1}{2}\alpha$ (i.e. the region between the points of discontinuous slope) for which $\mathrm{Im}(\sigma)$ is non-zero. The range of α_2 for which σ is complex decreases as μ approaches unity, where σ is real-valued everywhere. The root for $\mu = 0$ is shown by the dashed curve (this curve is covered on the right portion of the plot by the outermost solid curve). We again note that this branch is made up of two separate branches. However, in this case these roots *do not* intersect in the complex plane, and hence for small but non-zero values of μ these roots remain as two distinct roots. They later merge for larger values of μ.

Figure 6 shows the numerically computed roots for $\alpha = \pi$ as treated by Proudman & Asadullah (1988). The dashed curves (the one on the right portion of the graph is covered by the outermost solid curve) represent the solution for $\mu = 0$; the same as shown in figure 5 in Proudman & Asadullah (1988). Here we also show the roots for other values of μ. The stress in non-singular everywhere except for small values of μ and small values of α_2.

Figure 7 shows similar results for $\alpha = \frac{1}{2}\pi$. The insets show sketches of the flow for four different points on the solution curves for σ, and demonstrates the existence of the velocity and stress modes when Moffatt vortices are present. The upper-left inset corresponds to $\mu = 0.001$ and shows the velocity mode. Here the strength of the flow is comparable in each wedge. The upper-right inset corresponds to $\mu = 0.001$ and shows the stress mode. Here fluid 1 has a flow much weaker than that in fluid 2. The lower insets correspond to $\mu = 0.3$. There are still remnants of the two different modes in this case; however the lower-right inset now shows that the speeds in the two fluids are much less disparate than in the case where $\mu = 0.001$.

We can quantify the description of the singularities as follows. When $\alpha < \alpha_c$, where $\alpha_c \approx 0.715\pi$ ($\sin 2\alpha_c - 2\alpha_c \cos 2\alpha_c = 0$), the stress is never singular. When $\alpha_c < \alpha < \alpha_c + \pi$ the stress may or may not be singular depending on the individual wedge angles and the viscosity ratio. When $\alpha > \alpha_c + \pi$ the stress is always singular. The transition from the never singular case to the always singular case is shown in figure 8. Sketch (*b*) of this figure is a simplified version of figures 2–4 in Proudman &

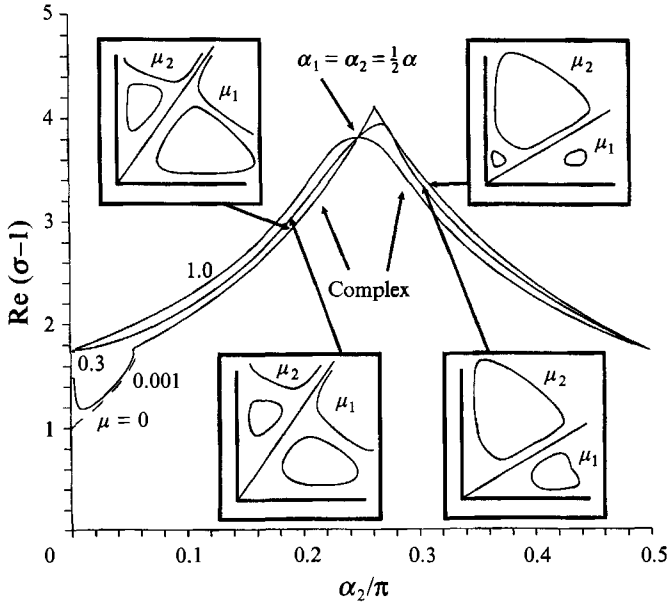

FIGURE 7. Partial local solutions: the two-fluid stress exponents for $\alpha = \frac{1}{2}\pi$ and various viscosity ratios, μ. The stress is never singular. The roots are complex everywhere except for small values of α_2 and small values of μ where the roots shown for $\mu = 0$ and $\mu = 0.001$ dip down. The roots shown for $\mu = 0.3$ and $\mu = 1$ are complex everywhere. The root shown for $\mu = 0$ is made up of two separate branches which *do not* intersect in the complex plane. Note the presence of the fixed point at $\alpha_1 = \alpha_2 = \frac{1}{2}\alpha$. The four insets correspond to points along the curves as indicated by the arrows. Here we see that the velocity and stress modes are present when Moffatt vortices occur. The stress mode for $\mu = 0.001$, sketched in the upper right inset, has a nearly static flow in fluid 1. However, the lower right inset, with $\mu = 0.3$, shows that for larger viscosity ratios the flow in fluid 1 strengthens.

Asadullah (1988) showing just the contour $\sigma = 1$. The shaded regions correspond to regions in parameter space where the stress is singular (i.e. $\mathrm{Re}(\sigma-1) < 0$) while the unshaded regions correspond to non-singular stresses (i.e. $\mathrm{Re}(\sigma-1) > 0$). The boundary between the two regions corresponds to $\mathrm{Re}(\sigma-1) = 0$ can be represented by

$$\mu = -\frac{(\sin 2\alpha_1 - 2\alpha_1 \cos 2\alpha_1)(\sin^2 \alpha_2 - \alpha_2 \sin \alpha_2 \cos \alpha_2)}{(\sin 2\alpha_2 - 2\alpha_2 \cos 2\alpha_2)(\sin^2 \alpha_1 - \alpha_1 \sin \alpha_1 \cos \alpha_1)}. \tag{3.9}$$

This is exactly the value of μ obtained if one solves (3.4) for μ. Therefore these boundaries also mark the location where stream functions with $\psi \sim r^2$ exist. Note that as this boundary is crossed there is in general a logarithmic singularity present in the stress which is due to the presence of the term θr^2 in the stream function. The same type of logarithmic singularity is found in the rigid/free single-fluid problem when σ crosses unity.

From these sketches we observe that for $\alpha_2 < \alpha_1$ (i.e. $\alpha_2 < \frac{1}{2}\alpha$) as μ increases σ increases and for $\alpha_2 > \alpha_1$ the reverse is true. This says that when the smaller of the two wedges corresponds to the less viscous fluid, the singularity is stronger than if the smaller wedge corresponds to the more viscous fluid.

We can similarly described the regions in parameter space where complex roots exist. We find that for $\alpha < 0.441\pi$ (this value corresponds to the value of α for which all of the roots of $\sigma \sin 2\alpha - \sin 2\sigma\alpha = 0$ are complex) the dominant root is always complex

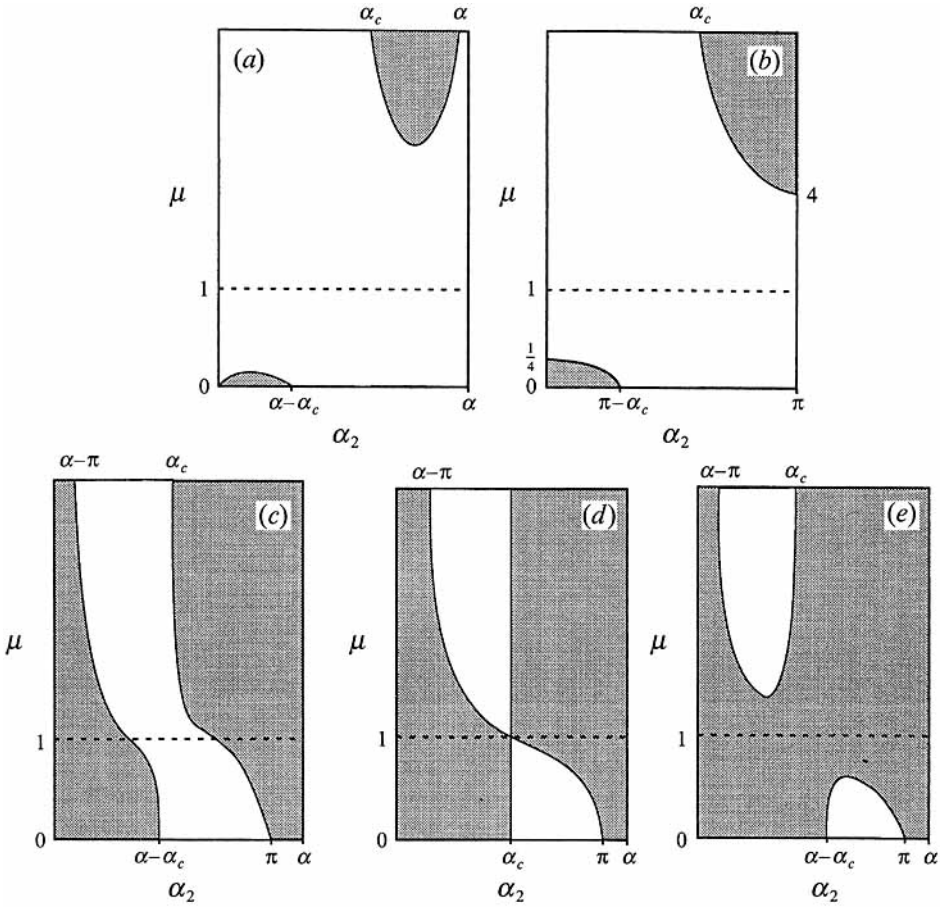

FIGURE 8. Partial local solutions: μ *vs.* α_2. The shaded regions correspond singular stresses ($\mathrm{Re}(\sigma-1)<0$) and the unshaded regions correspond to non-singular stresses ($\mathrm{Re}(\sigma-1)>0$). The five figures correspond to (*a*) $\alpha_c<\alpha<\pi$, (*b*) $\alpha=\pi$, see Proudman & Asadullah (1988), (*c*) $\pi<\alpha<2\alpha_c$, (*d*) $\alpha=2\alpha_c$, and (*e*) $2\alpha_c<\alpha<\alpha_c+\pi$, where α_c is the smallest positive solution of $\tan 2\alpha_c=2\alpha_c$, given approximately by 0.715π. Intercepts at $\mu=0$ are marked at the bottom of each figure while asymptotes for $\mu\to\infty$ are indicated along the top of each figure. For values of $\alpha<\alpha_c$ the stress is never singular and for values of $\alpha>\alpha_c+\pi$ the stress is always singular. Along the boundary separating the two regions there is in general a logarithmic singularity due to the presence of the term θr^2 in the stream function.

and for $\alpha>1.35\pi$ the dominant root is always real. Figure 9 shows the transition from always complex to never complex. The shaded regions correspond to $\mathrm{Im}(\sigma)\neq 0$ while the unshaded regions correspond to $\mathrm{Im}(\sigma)=0$ (for the dominant mode).

As in the single-fluid results, σ tends to decrease (leading to more singular stresses) as the total wedge angle gets larger. As noted by Proudman & Asadullah (1988), as either α_1 or α_2 approaches zero, the dominant mode has finite σ (e.g. compare figure 1 with figure 4).

We now consider local solutions. Michael & O'Neill (1977) have considered local solutions for the case $\mu=1$, which corresponds to single-fluid flow in a rigid/rigid wedge with the additional requirement that a separating streamline emanates from the corner. They found when the total wedge angle is π or 2π that the separating streamline can occur at *any* angle. For other wedges the streamline occurs only at specific angles

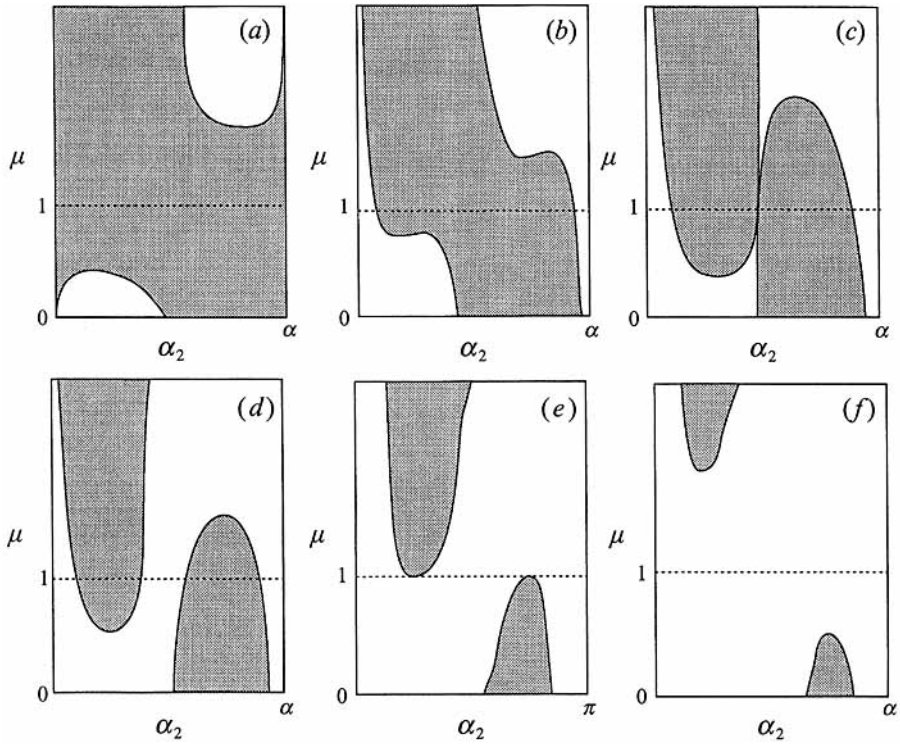

FIGURE 9. Partial local solutions: μ *vs.* α_2. The shaded regions correspond to $\mathrm{Im}\,(\sigma) \neq 0$ and the unshaded regions correspond to $\mathrm{Im}\,(\sigma) = 0$ (for the most dominant mode). The six figures correspond to (*a*) $0.441\pi < \alpha < 0.813\pi$, (*b*) $0.813\pi < \alpha < 0.884\pi$, (*c*) $\alpha = 0.884\pi$, (*d*) $0.884\pi < \alpha < \pi$, (*e*) $\alpha = \pi$, see Proudman & Asadullah (1988), and (*f*) $\pi < \alpha < 1.35\pi$. For values of $\alpha < 0.441\pi$ $\mathrm{Im}\,(\sigma)$ is always non-zero and for $\alpha > 1.35\pi$ it is always zero.

with the dominant mode (i.e. corresponding to the smallest value of $\mathrm{Re}\,(\sigma)$) having the separating streamline along the bisector of the wedge. The problem we pose reduces to that of Michael & O'Neill (1977) when the viscosity ratio $\mu = 1$.

For local solutions we must satisfy the normal-stress condition on the free surface, $\theta = 0$, (3.1*f*). This places another restriction on the parameters σ, α_2, α, and μ, namely

$$\frac{\alpha_2}{\alpha_1} F(\sigma\alpha_2)\,F(\alpha_2)\{F(2\alpha_1) - F(2\sigma\alpha_1)\} + \mu\cos\sigma\alpha_2\,F(\alpha_2)\{F^2(\alpha_1) - F^2(\sigma\alpha_1)\}$$

$$+ F^2(\alpha_1)\{\cos\alpha_2\,F(\sigma\alpha_2) - \cos\sigma\alpha_2\,F(\alpha_2)\} = 0. \quad (3.10)$$

The 'relabelling' symmetry is still present. The coefficients for the stream functions are still given by (3.6) with parameter values which satisfy (3.3) and (3.10). In the special case where $\alpha_1 = \alpha_2 = \pi$ and $\sigma = 1, 2, 3, 4, \ldots$ the additional restriction for the existence of local solutions is that $D_\sigma^{(1)} = \mu D_\sigma^{(2)}$, which leaves

$$\psi_1 = \mu\psi_2 = \mu r^{\sigma+1}\left\{2C_\sigma^{(2)}\sin\sigma\theta\sin\theta + \frac{2D_\sigma^{(2)}}{\sigma+1}(\sin\sigma\theta\cos\theta - \sigma\cos\sigma\theta\sin\theta)\right\}. \quad (3.11)$$

Also, when $\mu = 1$, additional local solutions can be found for $\alpha_1 = \alpha_2 = \alpha_c \approx 0.715\pi$ where $2\alpha_c\cos 2\alpha_c - \sin 2\alpha_c = 0$ and the stream functions are given by

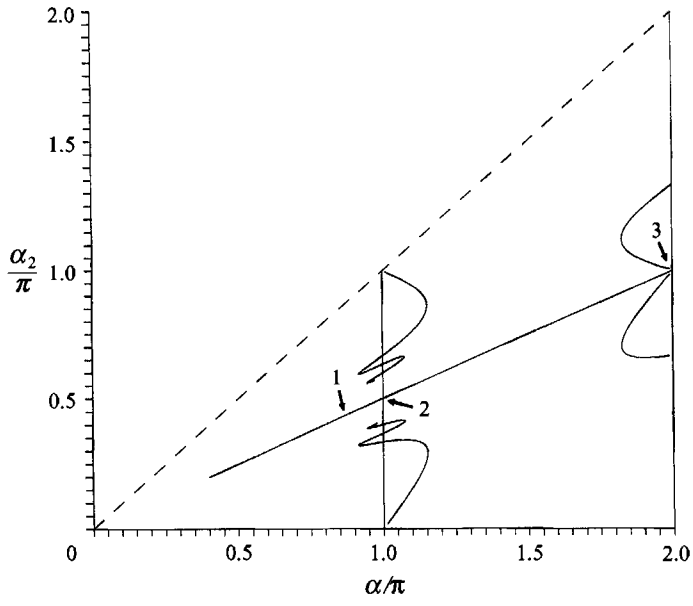

FIGURE 10. Local solutions: α_2 *vs.* α for $\mu = 1$. The vertical lines at $\alpha = \pi$, 2π and the line $\alpha_2 = \frac{1}{2}\alpha$ are solutions presented by Michael & O'Neill (1977). The other curves, not discussed by those authors, show that solutions exist for angles other than $\frac{1}{2}\alpha$ when $\alpha \neq \pi$, 2π but that they are not the dominant modes. Each branch shown here has a corresponding branch σ, which is shown in figure 11.

$$\tilde{\psi}_1 = r^{\sigma+1}\{A_\sigma^{(1)}\cos(\sigma+1)\theta + B_\sigma^{(1)}\sin(\sigma+1)\theta + C_\sigma^{(1)}\cos(\sigma-1)\theta + D_\sigma^{(1)}\sin(\sigma-1)\theta\} + B_1^{(1)}r^2\{(-2\cos 2\alpha_c)\theta + \sin 2\theta\}, \quad (3.12a)$$

$$\tilde{\psi}_2 = r^{\sigma+1}\{A_\sigma^{(2)}\cos(\sigma+1)\theta + B_\sigma^{(2)}\sin(\sigma+1)\theta + C_\sigma^{(2)}\cos(\sigma-1)\theta + D_\sigma^{(2)}\sin(\sigma-1)\theta\} + B_1^{(1)}r^2\{(-2\cos 2\alpha_c)\theta + \sin 2\theta\}, \quad (3.12b)$$

where the coefficients for the terms proportional to $r^{\sigma+1}$ are given by (3.6). Note that σ is determined by (3.3) and (3.10) with the parameter values $\alpha_1 = \alpha_2 = \alpha_c = \frac{1}{2}\alpha \approx 0.715$ and $\mu = 1$.

In order to determine the parameter values for which local solutions exist in the general case we must solve (3.3) and (3.10) simultaneously. We find that for a given value of μ we can obtain α_2 and σ as functions of α. Equivalently, for a fixed value of α we can obtain α_2 and σ as functions of μ (Anderson 1993). Recall that for single-fluid flow the rigid/rigid wedge has local solutions for all wedge angles while the rigid/free wedge has local solutions only for the specific wedge angle, π. In the two-fluid problem, depending on the value of μ there may or may not be local solutions for all wedge angles.

We have plotted the solutions σ and α_2 as functions of α for $\mu = 1$ (figures 10 and 11), $\mu = 0.9$ (figures 12–14), and $\mu = 0.02$ (figures 15 and 16). Note that each curve shown in the α_2 *vs.* α plane has a corresponding value of σ, shown plotted as $\mathrm{Re}(\sigma - 1)$ *vs.* α.

Figures 10 and 11 show the solutions for $\mu = 1$ as obtained by Michael & O'Neill (1977). The vertical lines $\alpha = \pi$ and 2π in figure 10 correspond to $\sigma = 2, 3, 4, \ldots$ at $\alpha = \pi$ and $\sigma = \frac{1}{2}, 1, \frac{3}{2}, \ldots$ at $\alpha = 2\pi$, respectively, in figure 11. The line $\alpha_2 = \frac{1}{2}\alpha$ in figure 10 corresponds to the values of σ satisfying $\sigma \sin\alpha - \sin\sigma\alpha = 0$ in figure 11. The dashed

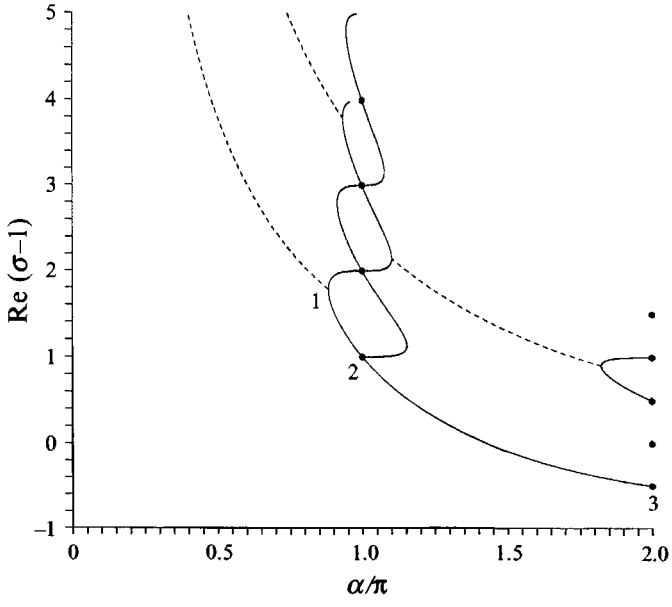

FIGURE 11. Local solutions: the values of σ which correspond to the solutions α_2 shown in figure 10. The curve which is the dominant mode (i.e. smallest value of $\mathrm{Re}\,(\sigma)$) as well as its extension to larger values of $\mathrm{Re}\,(\sigma)$ corresponds to the solution $\alpha_2 = \frac{1}{2}\alpha$ in figure 10. The points $\sigma - 1 = 1, 2, 3, 4, \ldots$ and the points $\sigma - 1 = -\frac{1}{2}, 0, \frac{1}{2}, \ldots$ correspond to the vertical lines at $\alpha = \pi$ and $\alpha = 2\pi$, respectively, in figure 10 (Michael & O'Neill 1977). Notice that two different curves for α_2 correspond to the same value of σ, consistent with the relabelling symmetry. For $\alpha < 0.884\pi$ the value of σ becomes complex along the dominant mode (dashed curve). Two other complex branches corresponding to solutions of $\sigma \sin\alpha - \sin\sigma\alpha = 0$ are shown.

curves represent solutions which have non-zero $\mathrm{Im}\,(\sigma)$. The complex branch emanating from the first turning point (point 1), at $\alpha = 0.884\pi$, represents the dominant mode for $\alpha < 0.884\pi$. The presence of these complex roots indicates that Moffatt vortices will be present in the two-fluid system when $\mu = 1$. Owing to the requirement of the presence of a separating streamline, this dominant mode is a higher-mode solution of the single-fluid, rigid/rigid wedge problem (compare figure 1). We identify additional solutions not discussed by Michael & O'Neill (1977). These solutions can be seen as the upper and lower curves near $\alpha = \pi$ in figure 10 each corresponding to the branch in figure 11 intertwined with the previously discussed branch. These upper and lower branches in figure 10 are actually mirror images reflected about the wedge bisector, $\alpha_2 = \frac{1}{2}\alpha$, and hence must necessarily correspond to the same value of σ. Note that there are also roots leaving the turning points of the higher-mode branch that is intertwined with the branch corresponding to the solutions of $\sigma \sin\alpha - \sin\sigma\alpha = 0$; however, these branches correspond to values of α_2 which are complex and hence are not physically allowable. The two branches in figure 10 extending into the domain for values of α near 2π correspond to the higher-mode solution near $\alpha = 2\pi$ in figure 11, and also have the same mirror symmetry. The existence of these higher-mode solutions indicates that angles other than $\alpha_2 = \frac{1}{2}\alpha$ are allowed when $\alpha \neq \pi, 2\pi$ but do not correspond to the dominant mode.

In order to describe the behaviour of these roots as μ is perturbed from unity, it is necessary to identify the singular points at $\mu = 1$, in particular the turning points and the double/multiple roots. There are several such points in parameter space; we shall

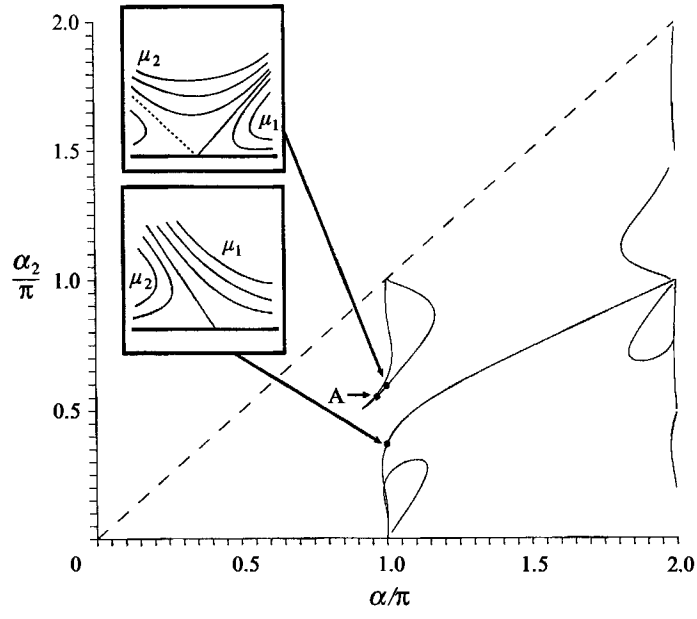

FIGURE 12. Local solutions: α_2 *vs.* α for $\mu = 0.9$. Near $\alpha = \pi$ the solution branches have bifurcated into separate branches. The branch for $\alpha < 0.884\pi$ has disappeared since the corresponding value of α_2 has become complex. The insets show the corresponding flow field for the points along the solution branches indicated by arrows. The lower inset shows a 'typical' first-mode flow while the upper inset shows a higher-mode flow in which there is a separating streamline present in fluid 2. Point A indicates the position along the upper branch in which the flow in fluid 2 develops a separating streamline; beginning to the right of this point and ending at $\alpha = \alpha_2 = \pi$ the flow is separated and beginning to the left and ending at $\alpha = \alpha_2 = \pi$ the flow is not separated. Point A corresponds to the local maximum in the value of σ as shown in figure 13.

focus on just three. These are points 1, 2 and 3 as shown in figures 10 and 11. Point 1 is a turning point; to the right corresponding to real-valued σ and to the left complex-valued σ. Point 2 corresponds to a double root ($\alpha = \pi$, $\alpha_2 = \frac{1}{2}\pi$, $\sigma = 2$). It is important to note that the point marked by 2 in figure 10 can be identified with any of the points $\sigma = 2, 3, 4, \ldots$ at $\alpha = \pi$ in figure 11. We shall only consider the point corresponding to the smallest value of σ. Point 3 is also a double root ($\alpha = 2\pi$, $\alpha_2 = \pi$, $\sigma = \frac{1}{2}$). We find that solutions to the system of nonlinear equations undergo several interesting bifurcations at these points when μ is perturbed from unity.

Figures 12–14 show the solutions for $\mu = 0.9$. We shall consider first the bifurcation from point 1 (see figures 10 and 11). The branch corresponding to complex values of σ, when $\mu = 1$ and $\alpha < 0.884\pi$, is *never* a solution for $\mu \neq 1$ because α_2 becomes complex along this branch and is therefore not physically allowable (compare figures 10 and 11 with figures 12 and 13). The complex 'root' is actually a pair of roots that leaves the physical plane when perturbed. This result was obtained numerically and confirmed by asymptotic analysis (Anderson 1993).

The second region of interest is near point 2 in figures 10 and 11 where the two branches (*a*) $\alpha = \pi$, $\sigma = 2$, and (*b*) $\alpha_2 = \frac{1}{2}\alpha$, $\sigma \sin\alpha - \sin\sigma\alpha = 0$ intersect. Notice that branch (*a*) is a solution for *all* values of $\alpha_2 < \pi$ but for a *single* value of σ and α, while branch (*b*) is a solution for *specific* values of α_2 and σ at each value of α. When μ is perturbed from unity, these two branches split at the intersection and form two non-intersecting branches. If we look at this bifurcation in the α_2 *vs.* α plane (figure 12), we

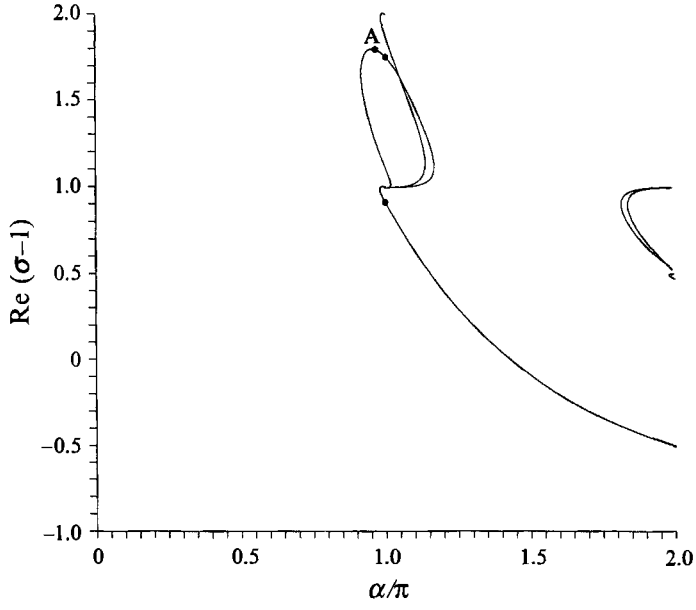

FIGURE 13. Local solutions: the values of σ which correspond to the solutions α_2 shown in figure 12. The branches which corresponded to a double root with complementary values of α_2 for $\mu = 1$ have now separated. There is also a small-scale pattern near $\alpha = \pi$ and $\sigma = 2$ which is enlarged in figure 14. All of the roots shown are real valued. Note that to the right of point A along this branch the flow is separated in fluid 2 while to the left it is not separated.

see that the lower portion of branch (*a*) has merged with the right portion (i.e. $\alpha > \pi$) of branch (*b*). The upper portion of branch (*a*) has merged with the left portion of branch (*b*).

Figure 13 shows this bifurcation in the $\mathrm{Re}(\sigma - 1)$ *vs.* α plane. The solution has not changed significantly from the $\mu = 1$ case for values of α significantly larger than π but near $\alpha = \pi$ the changes are quite dramatic. From this figure we see that the locally monotone curve with $\mu = 1$ near $\alpha = \pi$ and $\sigma = 2$ (see figure 11) has become multi-valued. Figure 14 shows the region near this point enlarged so that even more structure is revealed. Here we see that the solutions which corresponded to the 'single point' $\sigma = 2$, $\alpha = \pi$ and the curve passing through this point have bifurcated into a partial spiral pattern. This occurs on a very small scale that is present but only partially visible in figure 13. Note that for values of α just smaller than π there are now five values of σ near $\sigma = 2$ rather than the previous single value for $\mu = 1$.

The insets in figure 12 show sketches of the flow for points along the upper and lower bifurcated branches at $\alpha = \pi$. These points are also marked in figure 13. The lower inset corresponds to the lower branch and shows a 'typical' first-order corner flow. Point A shown in these figures indicates the position along the upper branch at which the flow in fluid 2 develops a separating streamline. For values along this curve beginning to the right of this point and ending at $\alpha = \alpha_2 = \pi$ and $\sigma = 2$ the flow in fluid 2 is separated. For values along this curve beginning to the left of this point and ending at $\alpha = \alpha_2 = \pi$ and $\sigma = 2$ neither of the flows in fluid 1 or fluid 2 is separated. The upper inset corresponds to a point along this higher mode in which there is a separating streamline in fluid 2.

We have captured the bifurcation near point 2 numerically as well as asymptotically. The uniformly valid solutions for α_2 and σ as functions of α for $\mu \sim 1$ which describes

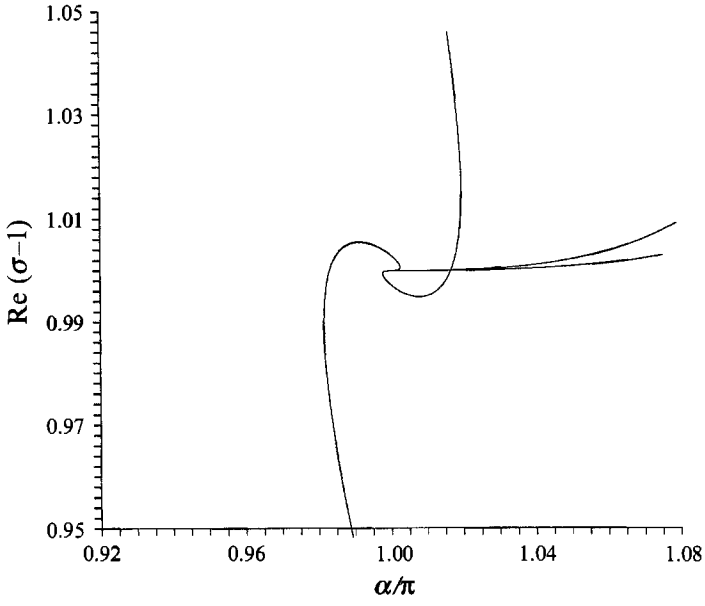

FIGURE 14. Local solutions: the blown up region near $\alpha = \pi$ and $\sigma = 2$ in figure 13 which shows how the two solution branches at $\mu = 1$ have bifurcated into a partial-spiral pattern. Similar patterns are present in other locations in parameter space.

the partial spiral pattern in figure 14 and the corresponding values of α_2 in figure 12 are given by

$$\alpha_2 \sim (\tfrac{1}{2}\alpha + \alpha_0(\xi) - \tfrac{1}{2}\pi) + \ldots, \tag{3.13a}$$

$$\sigma \sim \sigma_0(\alpha) + (\mu - 1)\frac{4}{\pi}\left(\xi - \frac{\sin^4 \alpha_0(\xi)}{\tan 2\alpha_0(\xi)}\right) + \ldots, \tag{3.13b}$$

where $\xi \equiv (\alpha - \pi)/(\mu - 1)$, $\alpha_0(\xi)$ is determined by

$$\xi = -4 \tan \alpha_0(\xi)\,(\sin^2 \alpha_0(\xi) - (\tfrac{1}{2} - \tfrac{1}{4}\sqrt{2}))\,(\sin^2 \alpha_0(\xi) - (\tfrac{1}{2} + \tfrac{1}{4}\sqrt{2})), \tag{3.14}$$

and $\sigma_0(\alpha)$ is determined by $\sigma_0 \sin \alpha - \sin \sigma_0 \alpha = 0$. This perturbation expansion is valid for the portion of the branch including the partial-spiral pattern seen in figure 14 and is matched to the outer solution in both directions but does not include the turning point region.

Next, we consider the region near point 3. The sections of the vertical line $\alpha = 2\pi$ with $\frac{1}{2}\pi < \alpha_2 < \pi$ and $\frac{3}{2}\pi < \alpha_2 < 2\pi$ in figure 10 begin to bow into the domain (see figure 12) for $\mu = 0.9$, while the other sections bow out of the physical domain as μ is perturbed from unity. The 'single point' $\sigma = \frac{1}{2}$ in figure 11 grows into curves which extend as far into the domain as the curves for α_2. These curves are barely visible here but become more apparent for values of μ farther from unity. These branches are very important since they correspond to the dominant mode for values of α near 2π.

Other solutions for $\mu = 0.9$ can be seen in figures 12 and 13. In particular we can observe the splitting of the two higher-mode solutions, σ, (compare figures 11 and 13) and the presence of a small lobe just underneath these modes in figure 13 near $\alpha = 2\pi$. Figure 12 shows the corresponding value of α_2.

In figures 15 and 16 some of these roots are shown for $\mu = 0.02$. The two roots on

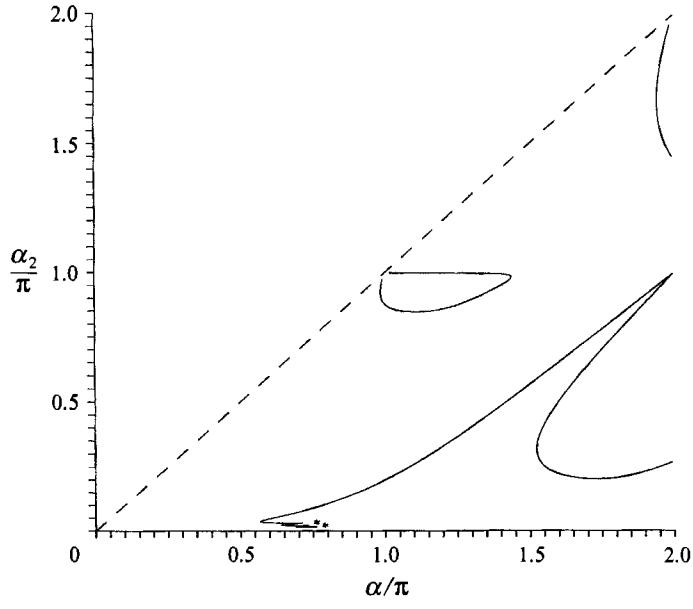

FIGURE 15. Local solutions: the first few roots for $\mu = 0.02$. The isolated points, marked by asterisks, correspond to solutions that have complex values of σ while still having real-valued solutions for α_2. Such complex solutions can be represented as a family of solutions with the free parameter α but, because μ is fixed, they appear on these plots as isolated points.

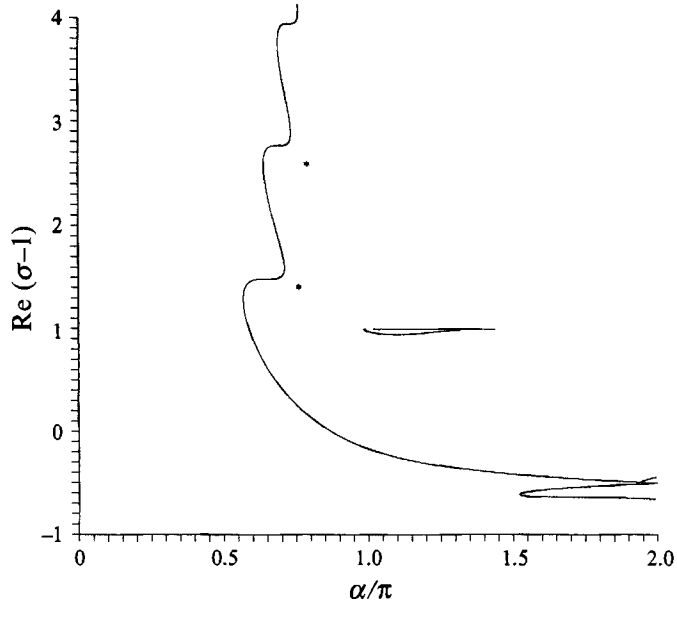

FIGURE 16. Local solutions: the values of $\mathrm{Re}\,(\sigma - 1)$ which correspond to the solutions α_2 shown in figure 15. The presence of the complex-valued solutions is indicated by the asterisks (only the real part is shown). All other values of σ on this plot are real valued. These isolated point solutions fall along complex branches connecting the real branches shown in this figure. However, along such branches the value of α_2 is complex except at the points shown, where its imaginary parts crosses zero.

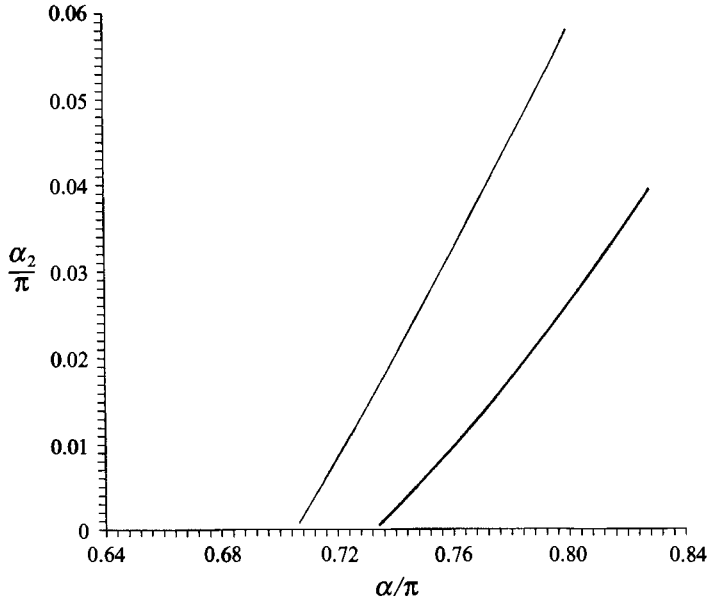

FIGURE 17. Local solutions: the value of α_2 corresponding to two roots which have complex values of σ. They correspond to very small values of α_2 and very small values of μ; however, by symmetry there are also solutions with α_2 very near α for large values of μ.

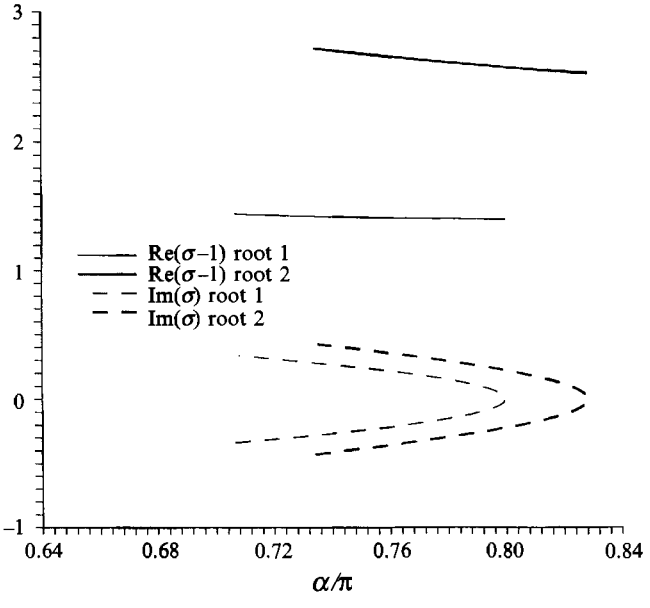

FIGURE 18. Local solutions: the real and imaginary parts of σ corresponding to two roots which have complex values of σ yet real values of α_2 and μ. They correspond to higher-mode solutions. These branches continue as real-valued solutions to the right but terminate on the left since the corresponding value of α_2 becomes negative.

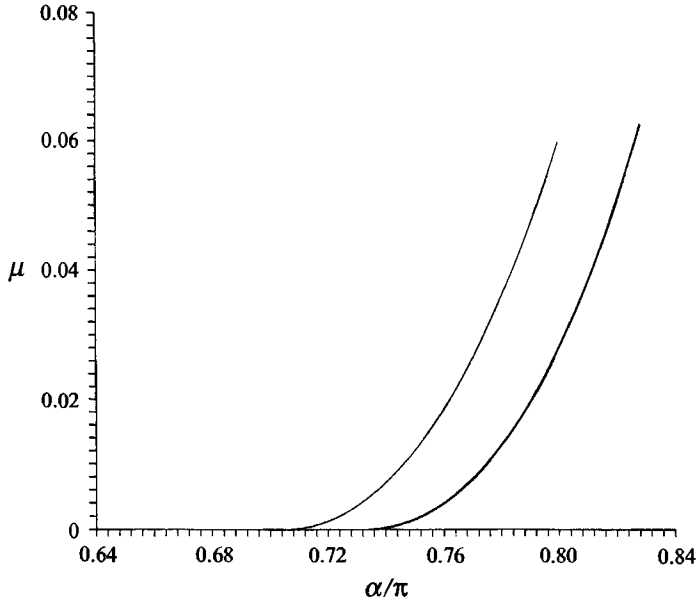

FIGURE 19. Local solutions: the values of μ corresponding to two roots that have complex values of σ. Notice that they correspond to very small values of μ, indicating very disparate fluid viscosities.

the right in figure 15 originate from the vertical line $\alpha = 2\pi$ for $\mu = 1$ in figure 10 and are now bowed-in significantly (the higher-mode solutions for $\mu = 1$ appearing near $\alpha = 2\pi$ in figures 10 and 11 are not shown here). We can see that this lower root is the dominant mode for large values of α. Therefore, there is a discontinuity in the dominant mode as α varies. The 'main' branch, with α_2 ranging from π down to zero and σ increasing from $\frac{1}{2}$, in figures 15 and 16 has evolved from the branches, $\alpha_2 = \frac{1}{2}\alpha$, $\alpha = \pi$, as well as the higher-mode solution shown near $\alpha = \pi$ and the corresponding values of σ for $\mu = 1$ in figures 10 and 11. These branches just discussed all have real values of σ.

The isolated points marked by asterisks in figures 15 and 16 correspond to solutions with complex values of σ (just the real parts are plotted). These points fall along branches which have, in general, complex values of σ and α_2. These isolated solutions correspond to points along these complex branches where $\mathrm{Im}(\sigma) \neq 0$ while $\mathrm{Im}(\alpha_2) = 0$ (i.e. where $\mathrm{Im}(\alpha_2)$ crosses zero). There is a one-parameter family of solutions with $\mathrm{Im}(\sigma) \neq 0$ and $\mathrm{Im}(\alpha_2) = 0$. The solutions with complex values of σ have one fewer degree of freedom than the solutions for real values of σ. To see this we note that regardless of whether σ is real or complex, we need to solve the two equations (3.3) and (3.10). When σ is real, there are four independent variables, σ, α_2, α, and μ, and therefore we expect to find a two-parameter family of solutions, namely $\alpha_2 = \alpha_2(\alpha, \mu)$ and $\sigma = \sigma(\alpha, \mu)$ as seen in figures 10–16. When σ is complex, say $\sigma = p + iq$, both (3.3) and (3.10) will have real and imaginary parts. This gives us four real equations to solve. However, since σ is the only complex parameter, there are only the five independent variables p, q, α_2, α, and μ. This leads to a one-parameter family of solutions, viz. $\alpha_2 = \alpha_2(\alpha)$, $\sigma = \sigma(\alpha)$, and $\mu = \mu(\alpha)$. Figures 17–19 show two such complex roots. Note that they correspond to very small values of α_2 and μ (by symmetry there are also solutions with α_2 near α and μ very large). These solutions appear as single points in figures 15 and 16 since the value of μ is fixed.

To the right of the 'main' branch there appear to be a sequence of complex roots as shown by the isolated points in figures 15 and 16. These points, however, appear for only a small window of parameter values. We find that when μ increases, the main branch of σ moves to the right (i.e. towards larger values of α). At the same time, the isolated complex solutions also move towards larger values of α as μ is increased (see figure 19). However, the main branch catches up to the complex points near $\mu = 0.06$ and incorporates them into the main branch as real solutions.

There do not appear to be solutions for values of α to the left of the main branch (i.e. smaller values of α) for $\mu \neq 1$. Recall that we found asymptotically that, when μ was perturbed from unity, the value of α_2 became complex along the dominant branch. We have tracked the complex roots which bifurcate to the left for the first few limit points of the main branch for values of μ ranging from near zero to near unity but find the value of α_2 along these branches is complex; no points where $\mathrm{Im}(\alpha_2)$ crosses zero similar to those found to the right of the main branch were found.

These results have revealed several quite different types of behaviour of the solution when μ is perturbed from unity. Firstly, near $\alpha = 2\pi$ we observe that 'new' branches can form and become the dominant mode (this feature is more apparent for smaller values of μ). Secondly, near the intersection at $\alpha = \pi$, $\alpha_2 = \frac{1}{2}\pi$, and $\sigma = 2$ the nature of the solution changes dramatically. We observe a splitting of the roots at this point. Finally, the most dramatic change occurs for $\alpha < 0.884\pi$ where the perturbed solution loses existence.

We note that for given values of α and μ there are many possible values of α_2 and σ for local solutions. These modes are relatively ordered in terms of the value of $\mathrm{Re}(\sigma)$ since the higher modes correspond to larger values of $\mathrm{Re}(\sigma)$. The domain for σ is unbounded and hence the roots can 'spread out'. However, all of these modes must correspond to values of α_2 between zero and α and hence as more and more modes are shown these plots become cluttered. It is therefore conceivable that for some values of μ and α almost any value of α_2 between zero and α, hence any geometry, is allowed. However, since the solutions come in pairs, (α_2, σ), we can identify those geometries that correspond to the most dominant mode.

4. Summary

We have presented a local picture of two-fluid flow in a wedge. The governing equations simplify to the biharmonic equation for the stream function, $\psi \sim r^{\sigma+1} f_\sigma(\theta)$. We give the geometries for which solutions exist, identify the types of singularities that are present at the corner, and determine how these singularities vary with the wedge angle. We have also identified cases where Moffatt vortices may be present.

The class of solutions sought are those with bounded velocities at the wedge vertex. We distinguish between local solutions, satisfying all local boundary conditions, and partial local solutions. Partial local solutions are studied when a free surface is present and satisfy all of the local boundary conditions except the normal-stress boundary condition. They represent the leading-order perturbation approximation for ψ for an asymptotic expansion for small capillary number, C. Section 2.1 contains a discussion of the perturbation theory taking into account the higher-order terms. We find that the limit $C \to 0$ with $r \to 0$ is non-uniform and that, in support of the results by Schultz & Gervasio (1990), the free surface has an infinite curvature at the corner that is balanced by the normal force exerted on it.

For single-fluid flow in a wedge defined by two rigid planes, local solutions exist for all wedge angles (Dean & Montagnon 1949). Local solutions can be obtained only for

the wedge angle π for both rigid/free (Michael 1958) and free/free wedges. For the rigid/free case the stress has a square-root singularity at the corner while in the free/free case the stress is regular. Partial local solutions (Moffatt 1964*a*) for rigid/free and free/free wedges can be found for all wedge angles. In general, as the wedge angle increases, $\mathrm{Re}(\sigma)$ decreases giving more singular stresses (see figure 1). When either one or both boundaries are rigid, Moffatt vortices are possible (Moffatt 1964*a*). In the rigid/free case, however, this is the case only for partial local solutions; local solutions with complex values of σ in such cases do not exist.

For two-fluid systems we have extended the analyses of Proudman & Asadullah (1988) and Michael & O'Neill (1977) to include all wedge angles and viscosity ratios for both local and partial local solutions. Here, the physical parameters are the two wedge angles, α_1 and α_2 (where $\alpha_1+\alpha_2=\alpha$), and the viscosity ratio, μ. In an analogous fashion to the single-fluid results with the rigid/free wedge, local solutions could be found only for specific wedge geometries; however, there now exists a class of geometries for which this is true. Given values of μ and α, the values of σ and α_2 (or α_1) can be determined. For partial local solutions there is an additional degree of freedom and therefore we obtain $\sigma=\sigma(\mu,\alpha_1,\alpha_2)$. As in the single-fluid cases, $\mathrm{Re}(\sigma)$ tends to increase as the total wedge angle decreases, however σ remains finite as either α_1 or $\alpha_2\to 0$. For $\alpha<0.715\pi$ the stress is never singular and for $\alpha>1.715\pi$ the stress is always so. Between these values the viscosity ratio and the individual wedge angles play a role in determining whether or not singularities are present. Further, when the smaller wedge of fluid corresponds to the lower viscosity, the singularity is stronger than otherwise. Also, for $\alpha<0.44\pi$ the dominant root is always complex while for $\alpha>1.35\pi$ it was always real.

An interesting feature of this analysis is the nonlinear behaviour of the roots, σ, for small but non-zero μ (or similarly large but finite μ) and also for μ near unity found for partial local solutions and local solutions.

For partial local solutions when $\mu=0$ there are distinct roots, σ, which have intersecting real parts. If these roots also intersect in the complex plane, then as μ increases from zero, these intersecting roots split and become distinct, non-intersecting roots (see figure 3). If these roots do not intersect in the complex plane, they remain as distinct, non-interacting roots when μ is perturbed from zero. These two roots correspond to the two modes of flow – velocity and stress – identified by Proudman & Asadullah (1988). We find that these modes are present for all total wedge angles, including those where Moffatt vortices are present, (e.g. when $\alpha=\frac{1}{2}\pi$).

For local solutions there is a similar nonlinear splitting of roots. Entire solution branches can be lost as the parameter are perturbed. Therefore, although solutions exist for all total wedge angles when $\mu=1$, not all total wedge angles admit solutions when $\mu\neq 1$.

In the analysis for local solutions we also find that higher-mode solutions (i.e. those with values of σ which were not the smallest) can become the dominant mode as parameter values changed (e.g. see figures 13 and 16).

We find that for both partial local solutions and local solutions σ can be complex, indicating that, as in the single-fluid cases, Moffatt vortices may be present. Local solutions with real values of σ are found as functions of α and μ, while those with complex values of σ comprise only a one-parameter family. Furthermore, local solutions with complex values of σ do not appear to correspond to the dominant mode except for the case where $\mu=1$.

The authors appreciate the suggestions on the numerical analysis by P. Gavin

LaRose. This work was supported by grants from the National Aeronautics and Space Administration through the Graduate Student Researchers Program (D.M.A.) and the Program on Microgravity Science and Applications (S.H.D.).

Appendix. Root-splitting asymptotics

We have performed a perturbation analysis which captures the root splitting bifurcation observed in the solutions of (3.3) required for the existence of partial local solutions for $\mu \ll 1$. The uniformly valid solution for $\mu \ll 1$ for the lower root is given by

$$\sigma \sim (\sigma_B + Z_0(\eta) - \sigma_0) + \mu^{\frac{1}{2}}\left(A(\xi) + \frac{2\sigma^* p_4}{p_1}\xi\right) + \ldots \quad \text{for } \alpha_2 < \alpha_2^*, \tag{A 1a}$$

$$\sigma \sim (\sigma_A + Z_0(\eta) - \sigma_0) + \mu^{\frac{1}{2}}\left(A(\xi) + \frac{\sigma^* p_3}{p_2}\xi\right) + \ldots \quad \text{for } \alpha_2 > \alpha_2^*, \tag{A 1b}$$

where
$$\sigma_B \sin 2\alpha_1 - \sin 2\sigma_B \alpha_1 = 0, \quad \sigma_A^2 \sin^2 \alpha_2 - \sin^2 \sigma_A \alpha_2 = 0 \tag{A 2a, b}$$

give the leading-order solution to the left and right of the intersection,

$$\eta \equiv \frac{\alpha_2}{\mu}, \quad \eta = \frac{4\sin^2 Z_0 \alpha - Z_0^2 \sin^2 \alpha}{Z_0(Z_0 \sin 2\alpha - \sin 2Z_0 \alpha)}, \quad \sigma_0 \sin 2\alpha - \sin 2\sigma_0 \alpha = 0 \tag{A 2c–e}$$

correspond to the inner boundary layer correction near $\alpha_2 = 0$, and

$$A(\xi) = \frac{-f_2 \xi \pm [(f_2^2 - 4f_1 f_4)\xi^2 - 4f_1 f_3]^{\frac{1}{2}}}{2f_1}, \quad \xi \equiv \frac{\alpha_2 - \alpha_2^*}{\mu^{\frac{1}{2}}} \tag{A 2f, g}$$

correspond to the inner solution near the intersection, σ^*, α_2^*, and α_1^* given by

$$\sigma^{*2} \sin^2 \alpha_2^* - \sin^2 \sigma^* \alpha_2^* = 0, \quad \sigma^* \sin 2\alpha_1^* - \sin 2\sigma^* \alpha_1^* = 0 \tag{A 2h, i}$$

$$f_1 = p_1 p_2, \quad f_2 = \sigma^*(p_1 p_3 + 2p_2 p_4), \quad f_3 = p_3 p_5, \quad f_4 = 2\sigma^{*2} p_3 p_4, \tag{A 2j–m}$$

$$p_1 = \sin 2\alpha_1^* - 2\alpha_1^* \cos 2\sigma^* \alpha_1^*, \quad p_2 = 2\sigma^* \sin^2 \alpha_2^* - \alpha_2^* \sin 2\sigma^* \alpha_2^*, \tag{A 2n, o}$$

$$p_3 = \sigma^* \sin 2\alpha_2^* - \sin 2\sigma^* \alpha_2^*, \quad p_4 = \cos 2\sigma^* \alpha_1^* - \cos 2\alpha_1^*, \quad p_5 = \sigma^{*2} \sin^2 \alpha_1^* - \sin^2 \sigma^* \alpha_1^*. \tag{A 2p–r}$$

We note that (A 2f) gives the correct inner expansion near a general intersection represented by σ^*, α_1^*, and α_2^* for both the upper and lower roots. The matching conditions determine which sign in (A 2f) is used. For the dominant branch (i.e. corresponding to the smallest value of σ) the minus sign in (A 2f) is always used. The range of α for which the lowest roots intersect is given approximately by $1.35\pi < \alpha < 2\pi$. We find good agreement between these asymptotic results and the numerical results for small values of μ.

REFERENCES

ANDERSON, D. M. 1993 PhD. thesis, Northwestern University.

BROWN, R. A. 1991 *IMA Meeting, Free Boundaries in Viscous Flows, Minneapolis.*

DAVIS, S. H. 1983 *Trans. ASME* E: *J. Appl. Mech.* **50**, 977–982.

DEAN, W. R. & MONTAGNON, P. E. 1949 *Proc. Camb. Phil. Soc.* **45**, 389–394.

DUSSAN, V., E. B. & DAVIS, S. H. 1974 *J. Fluid Mech.* **65**, 71–95.

HASIMOTO, H. & SANO, O. 1980 *Ann. Rev. Fluid Mech.* **12**, 335–363.

MICHAEL, D. H. 1958 *Mathematika* **5**, 82–84.
MICHAEL, D. H. & O'NEILL, M. E. 1977 *J. Fluid Mech.* **80**, 785–794.
MOFFATT, H. K. 1964*a* *J. Fluid Mech.* **18**, 1–18.
MOFFATT, H. K. 1964*b* *Arch. Mech. Stosowanej* **16**, 365–372.
PAN, F. & ACRIVOS, A. 1967 *J. Fluid Mech.* **28**, 643–655.
PROUDMAN, I. & ASADULLAH, M. 1988 *J. Fluid Mech.* **187**, 35–43.
SCHULTZ, W. W. & GERVASIO, C. 1990 *Q. J. Mech. Appl. Maths* **43**, 407–425.
RICHARDSON, S. 1970 *Proc. Camb. Phil. Soc.* **67**, 477–489.
TROGDON, S. A. & JOSEPH, D. D. 1981 *Rheol. Acta.* **20**, 1–13.